

Molecular Modeling and *In Vitro* Evaluation of Thioureas and Arylthioureas as Urease Inhibitors

Published as part of ACS Omega special issue "Chemistry in Brazil: Advancing through Open Science."

Marciéli Fabris, Priscila G. Camargo, Mariana L. Silva, Camilo H. S. Lima, Magaly G. Albuquerque, Carlos R. Rodrigues, Nailton M. Nascimento-Júnior, and Marcelle L. F. Bispo*



Cite This: *ACS Omega* 2025, 10, 21795–21812



Read Online

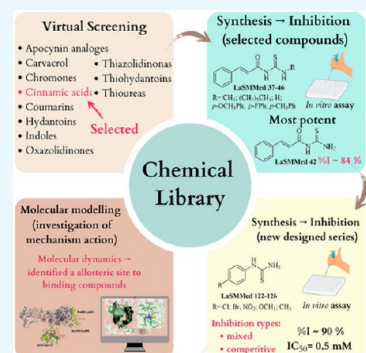
ACCESS |

Metrics & More

Article Recommendations

Supporting Information

ABSTRACT: Ureases are metalloenzymes found in plants, algae, fungi, and bacteria that are responsible for hydrolyzing urea into carbamate and ammonia. The bacterium *Helicobacter pylori*, which is associated with gastrointestinal disorders, produces large amounts of urease to neutralize stomach acidity. The rising antibiotic resistance of *H. pylori* presents a significant challenge for eradication efforts, highlighting the need for novel therapeutic strategies. In this study, we explored the LaSMMed chemical library to identify new urease inhibitors. Virtual screening identified six thioureas derived from cinnamic acid (LaSMMed 37–46), demonstrating urease inhibition rates ranging from 13% to 82%. The most potent compound, LaSMMed 42 ($\%I = 82\%$), was selected as a lead structure for designing a new series of arylthioureas (LaSMMed 122–126). These derivatives exhibited impressive inhibitory activity, with 84% and 88% inhibition rates. Their IC_{50} values ranged from 0.464 to 0.575 mM, and their inhibition constants (k_i) were between 0.080 and 0.130 mM, indicating competitive inhibition for LaSMMed 125 and mixed-type inhibition for LaSMMed 122–124 and LaSMMed 126. Molecular modeling studies provided insights into the structure–activity relationships and potential binding interactions, supporting their role as promising candidates for the development of new urease-targeting agents.



1. INTRODUCTION

Ureases are a type of metalloenzyme that belongs to the enzyme families amidohydrolase and phosphodiesterase. Their exclusive use of Ni^{2+} ions within their active sites sets them apart from other metal-dependent hydrolases. Ureases can be found in various organisms such as plants, algae, fungi, and bacteria. However, they are not present in animals.¹ These enzymes hydrolyze urea to form carbamate and ammonia.²

Ureases play critical roles in pathogen survival and virulence. Interestingly, ureases found in various microorganisms and plants exhibit significant similarity, despite their polypeptide chain composition differences. The catalytic amino acid residues of vegetal urease from *Canavalia ensiformis* (CEU), H407, H409, K490, H492, H519, H545, and D633, were found to be identical to their respective equivalents in bacterial urease *Helicobacter pylori* (HPU).³

H. pylori is a bacterium that can colonize the human stomach and cause various gastrointestinal problems. It adapts to the harsh stomach environment by producing a significant amount of urease that neutralizes pH levels.⁴ *H. pylori* infection is a significant global health concern, particularly in low-income regions, and is associated with an increased risk of gastric cancer.^{5–7} Eradicating *H. pylori* is challenging because of antibiotic resistance, which requires the development of innovative treatment strategies. Our research group has

developed several planned compounds using medicinal chemistry strategies. The LaSMMed chemical library contains over 300 diverse compounds, including coumarins, indoles, chromones, carvacrol derivatives, cinnamic acid derivatives, oxazolidinones, thiazolidinones, apocynin derivatives, hydantoins, thiohydantoins, and thioureas (Figure 1). These compounds are potential pharmacophoric groups for various biological activities, including antibacterial,^{8,9} anticancer,¹⁰ antiparasitic,^{11–14} antifungal,¹⁵ antioxidant,¹⁶ or anticholinesterase inhibition.¹⁷ In addition, we recently reported compounds such as coumarins,¹⁸ thiohydantoins, and hydantoins¹⁹ as potent inhibitors against *C. ensiformis* urease. We chose the LaSMMed chemical library for virtual screening because its compounds exhibit notable biological activity with at least one subunit linked to antimicrobial effects. We aim to identify potential hits that inhibit bacterial ureases in pathogenic microorganisms like *H. pylori*. In this study, we identified potential hits from the LaSMMed chemical library

Received: February 21, 2025

Revised: May 13, 2025

Accepted: May 15, 2025

Published: May 22, 2025



ACS Publications

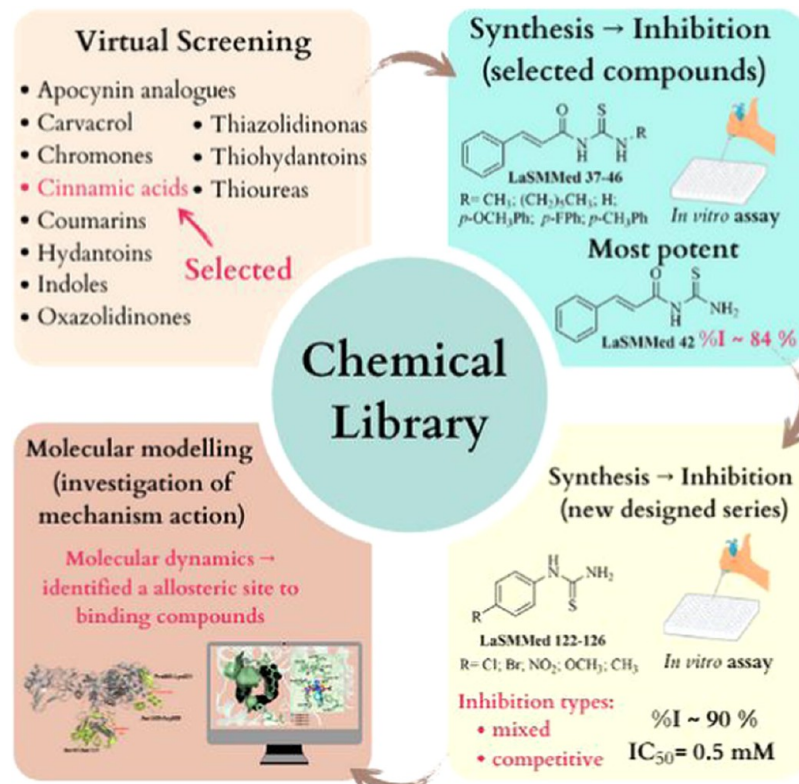


Figure 1. Structural design, experimental, and *in silico* approaches were applied to evaluate LaSMMed 37–46 and LaSMMed 122–126 derivatives as potential urease inhibitors.

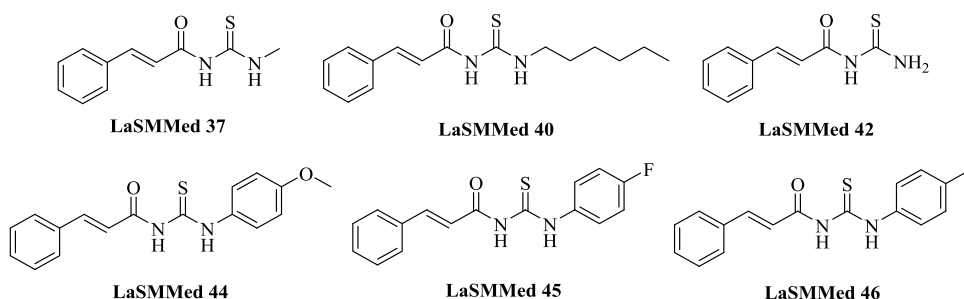


Figure 2. Substances from the LaSMMed chemical library were selected in the virtual screening process as possible *H. pylori* urease inhibitors.

and then synthesized and assessed the *in vitro* antiureolytic activity. Additionally, we designed and synthesized a new series of five arylthioureas with characteristics that enhance urease inhibition. The new series underwent evaluation *in vitro* for its inhibitory potential and mechanism of action. Finally, we conducted molecular modeling studies to gain insights into the structural activity relationship of this compound class (Figure 1).

2. RESULTS AND DISCUSSION

2.1. Virtual Screening on *H. pylori* Urease. The 3D structure of *H. pylori* urease (HPU, PDB ID: 6ZJA) used in our studies has a cocrystallized inhibitor of the hydroxycarbamide class (DJM), with a molecular volume of 244.12 Å³. We made the virtual screening of 130 substances (Table S1) available in our in-house chemical library, which has a molecular volume ranging from 90.25 to 280.06 Å³. The selection criteria for our substances were based on their interactions with key residues K219, H221, H248, A278, G279,

M317, C321, H322, M366, and I467(R), involved in interactions with DJM and with the catalytic Ni²⁺ ions (Ni601 and Ni602) (Tables S2–S15).

Our findings revealed that six substances from the LaSMMed chemical library interacted with 9 or 10 of the above-mentioned key residues from HPU. These substances are derivatives of *trans*-cinnamic acid, differing structurally due to the aliphatic groups (LaSMMed 37, 40, and 42) or the -4-substituted benzene rings (LaSMMed 44, 45, and 46) containing electron-donating (methoxy or methyl) or withdrawing groups (fluorine). All of them are characterized by a common thiourea subunit in their structures (Figure 2).

In general, all selected substances interacted with both Ni²⁺ ions and formed crucial hydrogen interactions with K221, a modified lysine pivotal for enzymatic activity,²⁰ as well as H221 and H248 histidines, which are located close to the center of the active site. Additionally, all compounds interacted with residues H136, H138, A169, H247, L318, and D362.

The *trans*-cinnamic acid derivatives LaSMMed 37, 40, and 42 with aliphatic substituents made conventional hydrogen

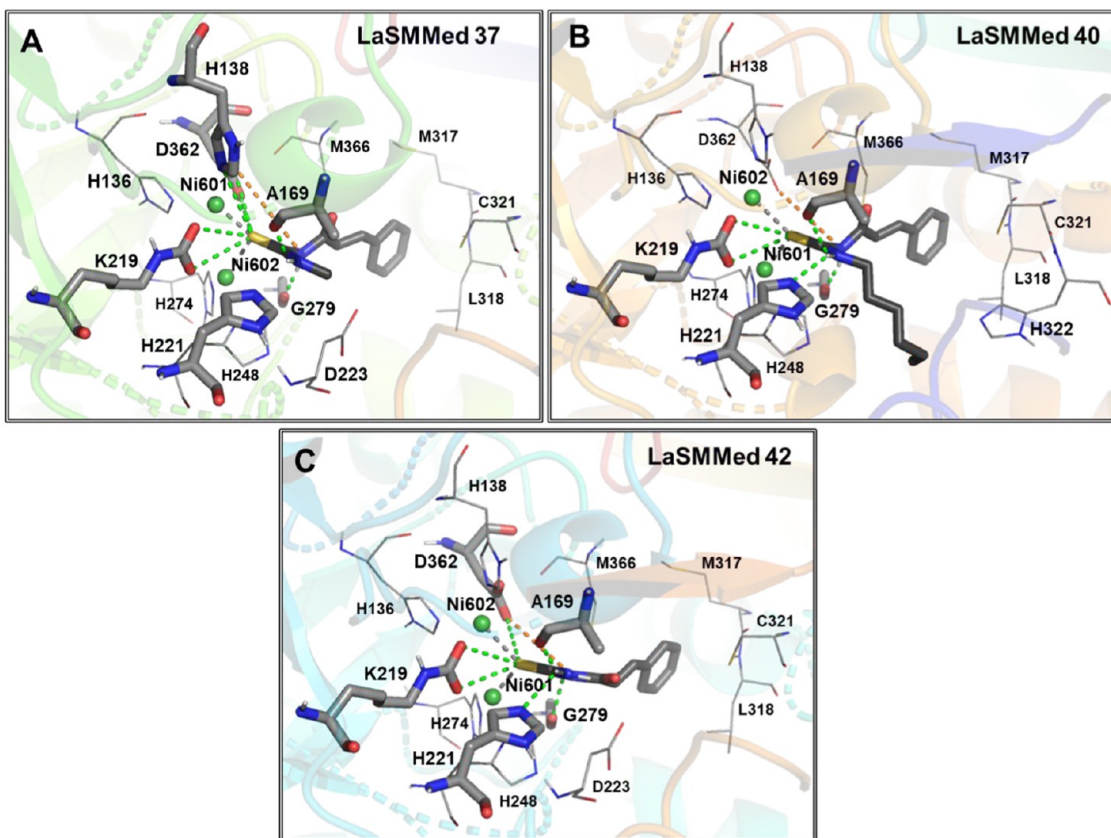


Figure 3. Interactions of the substances (A) LaSMMed 37, (B) 40, and (C) 42 with HPU. The gray sticks represent residues involved in hydrogen bonding, and the lines represent hydrophobic ones. Hydrogen bonds or π -S are shown by dashed green lines and π -alkyl in orange lines.

bonds with A169, K219, H221, and G279. Electrostatic interactions of the sulfur in the thiourea subunit with the imidazole ring from H136, H138, H221, and H248, along with metal–acceptor interactions between nickel ions and sulfur, were also present for all substances (Figure 3A–C). Minor interaction differences were observed for LaSMMed 37, 40, and 42. LaSMMed 203 approached H138, enabling a hydrogen bond interaction (S-HN) at 3.4 Å (Figure 3A). LaSMMed 37 distanced itself from D362, losing the hydrogen bond interaction but generating a hydrophobic interaction type π -alkyl between H322 and the hexyl CH (Figure 3A). LaSMMed 42 closely resembled LaSMMed 37, with the most significant difference being the loss of the hydrogen bond interaction with H138 (Figure 3C).

Thioureas featuring aromatic substituents LaSMMed 44, 45, and 46 exhibited interactions similar to those highlighted for aliphatic ones. However, the phenyl subunit in the substances contributed more to ligand–protein complementarity, allowing electrostatic interactions with residues D223 (π -anion) and A169 (π -alkyl) (Figure 4A–C).

LaSMMed 44 established a hydrogen bond (S-HN) with H138 at a distance of 2.9 Å (Figure 4A). LaSMMed 45 featured a π -S interaction between the benzene ring of the *trans*-cinnamic acid subunit and the sulfur of M317, along with a π -alkyl interaction with the carbon chain of M366 (Figure 4B). LaSMMed 46 adopted a pose allowing for a π -S interaction between the benzene ring and the sulfur of M366, along with a π -alkyl interaction with M317, L318, and C321 (Figure 4C). It was also observed for LaSMMed 44. The inclusion of a fluorine atom in LaSMMed 45 facilitated a halogen interaction with the nitrogen of H322, which served as

a Lewis base. In contrast, the other derivatives exhibited a π -alkyl interaction between the imidazole of H322 and the methyl present in the ligands (LaSMMed 44 and 46).

2.2. Synthesis of LaSMMed 37–46 Derivatives Identified by Virtual Screening. The synthesis of six thioureas derived from cinnamic acid (LaSMMed 37–46) was conducted using a methodology previously described by our research group.²¹ This process involved three steps carried out in a one-pot protocol, where primary amines were reacted with cinnamoyl isothiocyanate. First, the *trans*-cinnamic acid chloride was synthesized (Table 1, step a). Next, ammonium thiocyanate was added to form the corresponding cinnamoyl isothiocyanate (Table 1, step b). Finally, the appropriate primary amine was introduced into the reaction medium, resulting in the desired thioureas (LaSMMed 37–46) with yields ranging from 62 to 90% (Table 1, step c).

The structures of LaSMMed 37–46 derivatives were confirmed through ¹H and ¹³C NMR analyses (Figures S1–S9, Supporting Information). In the ¹H NMR spectra, characteristic signals indicated the presence of products: an NH singlet appeared between 8.5 and 10 ppm, while the α and β carbonyl hydrogens were observed as doublets at 6.5–7.0 and 7.5–8.0 ppm, respectively. Additionally, the methine hydrogens of benzene rings were detected in the range of 7.0–8.0 ppm. The ¹³C NMR spectra displayed α,β -carbon signals at 120 and 145 ppm, aromatic carbons above 110 ppm, and quaternary carbons between 180 and 170 ppm.

2.3. Antireolytic Activity of the LaSMMed 37–46 on *C. ensiformis* Urease. The compounds LaSMMed 37–46, which were selected during the virtual screening process, underwent the indophenol reaction to assess their potential to

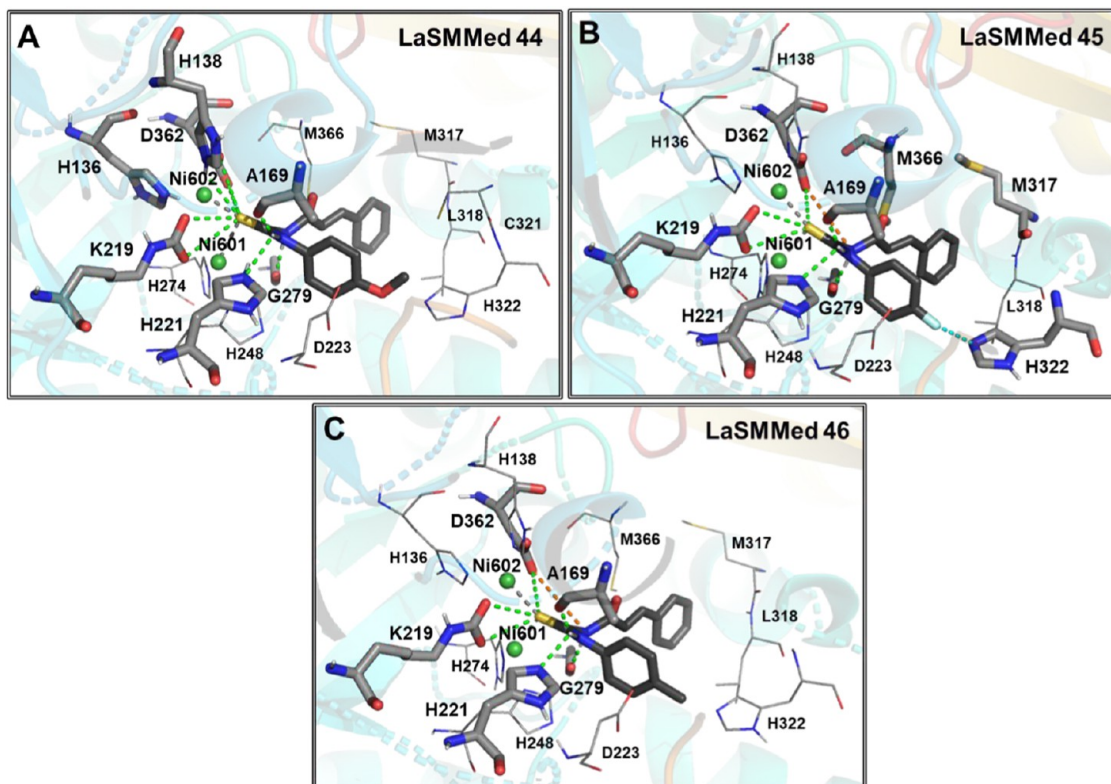
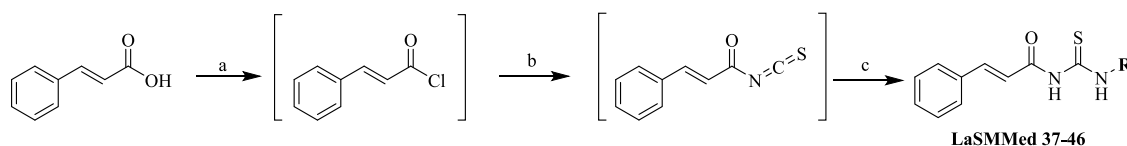


Figure 4. Interactions of the substances (A) LaSMMed 44, (B) 45, and (C) 46 with HPU. The gray sticks represent residues involved in hydrogen bonding, and the lines represent hydrophobic ones. Hydrogen bonds or π -S are shown by dashed green lines, halogen interaction is shown in cyan, and π -alkyl is shown in orange lines.

Table 1. Results of the Synthesis of Thioureas Derived from Cinnamic Acid LaSMMed 37, 40, 42, 44, 45, and 46



Conditions: (a) SOCl_2 , DMF, CH_2Cl_2 , reflux, 3 h. (b) NH_4SCN , acetone, reflux, 15 min. (c) RNH_2 , acetone, r.t., 40 min.

compound	R	yield (%)
LaSMMed 37	CH_3	69
LaSMMed 40	Hexyl	62
LaSMMed 42	H	74
LaSMMed 44	$4-\text{OCH}_3\text{Ph}$	75
LaSMMed 45	$4-\text{FPPh}$	72
LaSMMed 46	$4-\text{CH}_3\text{Ph}$	90

inhibit the enzymatic activity of *C. ensiformis* urease (CEU). This highly purified commercial urease is commonly used for *in vitro* experiments.²² Among the substances evaluated, the monosubstituted derivative LaSMMed 42 showed an impressive CEU inhibition of 82%, which was statistically comparable to the thiourea standard that also achieved 84% inhibition (Table 2). The disubstituted cinnamic acid derivatives, LaSMMed 37 and 40, both with aliphatic substituents, demonstrated moderate inhibition percentages (%) ranging from 30% to 40%. Notably, fluorine- and chlorine-substituted cinnamic acid derivatives have been shown to exhibit variable bioactivity depending on their substitution patterns,²³ which may explain the divergent inhibition rates observed here. In contrast, aromatic derivatives LaSMMed 45 (4-FPh) and 46

(4-CH₃Ph) displayed lower inhibition rates of 24 and 13%, respectively (Table 2). Additionally, compound LaSMMed 44 was insoluble under the tested conditions, preventing it from being analyzed (Table 2).

The results of the structure–activity relationship indicate that the primary thiourea subunit (without substituents) may freely enter the enzyme’s active site, interacting with Ni^{2+} ions and key amino acid residues. This interaction inhibits urea catalysis and ammonia release. As a result, due to its chemical structure, LaSMMed 42 shows promise as a prototype substance for designing new inhibitors. Accordingly, we propose designing a new small series of five arylthioureas that can serve as urease inhibitors, and we synthesized them to validate this hypothesis.

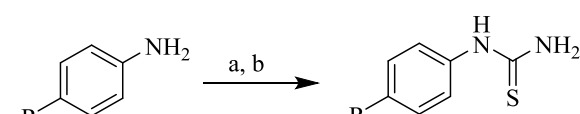
Table 2. Inhibitory Percentage (%I) of LaSMMed 37–46 and Standard Thiourea against CEU^a

LaSMMed 37–46	R	%I ± SD
LaSMMed 37	CH ₃	33.53 ± 1.06 ^c
LaSMMed 40	(CH ₂) ₅ CH ₃	39.34 ± 1.72 ^c
LaSMMed 42	H	82.37 ± 0.34 ^d
LaSMMed 44	4-OCH ₃ Ph	Nd
LaSMMed 45	4-FPh	23.98 ± 1.44 ^e
LaSMMed 46	4-CH ₃ Ph	13.04 ± 2.46 ^f
Thiourea	-	84.12 ± 0.84 ^d

^aSD: standard deviation of experiments performed in triplicate; Nd: not determined (insoluble). Different letters indicate a significant difference between values using the Scott–Knott test ($P < 0.05$).

2.4. Synthesis and Characterization of Arylthioureas

LaSMMed 122–126. We synthesized a concise set of monosubstituted arylthioureas (**LaSMMed 122–126**) by incorporating groups with varying stereochemical characteristics at the 4-position of the benzene ring. Initially, the respective aniline reacted with concentrated hydrochloric acid (Table 3, step a). Following this, a solution of ammonium

Table 3. Results of the Synthesis of Arylthioureas LaSMMed 122–126**LaSMMed 122–126**

Conditions: (a) HCl, 10 min; (b) NH₄SCN, H₂O, r.t., reflux, 24 h.

compound	R	yield (%)
LaSMMed 122	Cl	35
LaSMMed 123	Br	50
LaSMMed 124	NO ₂	38
LaSMMed 125	OCH ₃	48
LaSMMed 126	CH ₃	46

thiocyanate was added to the reaction mixture, forming arylthiourea derivatives **LaSMMed 122–126** with yields ranging from 38 to 48% (Table 3, step b).

The substances were characterized by using ¹H and ¹³C NMR spectroscopy (Figure S10–S13). Characteristic signals include a singlet at 9.5–10.3 ppm indicating disubstituted NH, as well as four aromatic hydrogens between 7.0 and 7.5 ppm. Additionally, a singlet at 3.5 ppm was observed, which is characteristic of primary amine hydrogens. In the ¹³C NMR spectra, signals were noted at 180 ppm, which are typical for carbonyls and thiones, along with aromatic methine CH signals ranging from 110 to 140 ppm.

2.5. Antiureolytic Activity of the LaSMMed 122–126 on *C. ensiformis* Urease. The results from the enzyme inhibition tests on the CEU assay indicate that arylthiourea derivatives exhibit excellent urease inhibitory potency, with inhibition percentages nearing 90% (Table 4). The derivatives **LaSMMed 122–126** and **LaSMMed 126** showed no statisti-

Table 4. Inhibitory Activity (%I) and IC₅₀ (mM) of LaSMMed 122–126 and Standard Thiourea against CEU^a

LaSMMed	R	%I ± SD	IC ₅₀ ± SD
LaSMMed 122	Cl	87.63 ± 1.72 ^a	0.575 ± 0.010 ^b
LaSMMed 123	Br	86.18 ± 0.75 ^a	0.493 ± 0.007 ^c
LaSMMed 124	NO ₂	88.30 ± 0.26 ^a	0.464 ± 0.003 ^d
LaSMMed 125	OCH ₃	84.56 ± 1.23 ^b	0.510 ± 0.019 ^c
LaSMMed 126	CH ₃	87.86 ± 0.48 ^a	0.568 ± 0.022 ^b
Thiourea	-	84.12 ± 0.84 ^b	0.504 ± 0.025 ^c

^aIC₅₀: half-maximum inhibitory concentration. SD: standard deviation of experiments performed in triplicate. Different letters indicate a significant difference between values using the Scott–Knott test ($P < 0.05$).

cally significant differences, suggesting that the substitutions on the benzene ring did not affect the antiureolytic activity within this series (Table 4). However, the derivative **LaSMMed 125**, which contains a powerful electron-donating group (OCH₃), demonstrated a notable difference in its inhibition value of 84% compared to the other derivatives, but it was statistically equal to that of the standard thiourea (Table 4). Notably, nitrogen-containing heterocycles (e.g., flavonoid analogues) have shown that electronic and steric modifications to the B-ring can significantly influence enzyme binding affinity, which may explain the enhanced activity of **LaSMMed 124** (NO₂-substituted) compared to other derivatives.²⁴

We also assessed the potency of derivatives by determining their half-maximum inhibitory concentration (IC₅₀). Among the arylthioureas, the nitro-substituted derivative **LaSMMed 124** exhibited the highest enzymatic inhibition, with an IC₅₀ of 0.464 mM, outperforming the standard thiourea (IC₅₀ = 0.504 mM). **LaSMMed 123** and **125** exhibited IC₅₀ values that were statistically comparable to those of thiourea (Table 4). In contrast, the arylthioureas with chloro and methyl substituents, **LaSMMed 122** and **126**, demonstrated the lowest inhibitory potency for CEU, with IC₅₀ values nearing 0.575 mM (Table 4).

We investigated the mechanism of action of **LaSMMed 122–126** derivatives using Lineweaver–Burk plots to determine the inhibition constant values (K_i), which are calculated from the slopes of each line graph. The results of Lineweaver–Burk plots indicate that, except for **LaSMMed 125**, which acts as a competitive inhibitor (Figure 4D), all other substances demonstrate mixed inhibition against CEU. This is evident from the graphs, where there is interception at different points on the Y-axis in the second quadrant of the X-axis²⁵ (Figure 5A–C and E).

The derivatives demonstrated V_{max} values ranging from 732 to 741 μmol of NH⁺ per minute per milligram of protein, while K_m values ranged from 0.65 to 0.67 mM (Table 5). Among the evaluated substances, **LaSMMed 125** demonstrated the highest affinity for urease with a K_i of 0.08 mM, closely followed by **LaSMMed 122** that had a K_i of 0.09 mM. In contrast, **LaSMMed 123**, **124**, and **126** all showed similar K_i values of 0.100 mM (Table 5).

In addition, the α parameter was calculated for all mixed inhibitors (**LaSMMed 122–124** and **LaSMMed 126**), and the

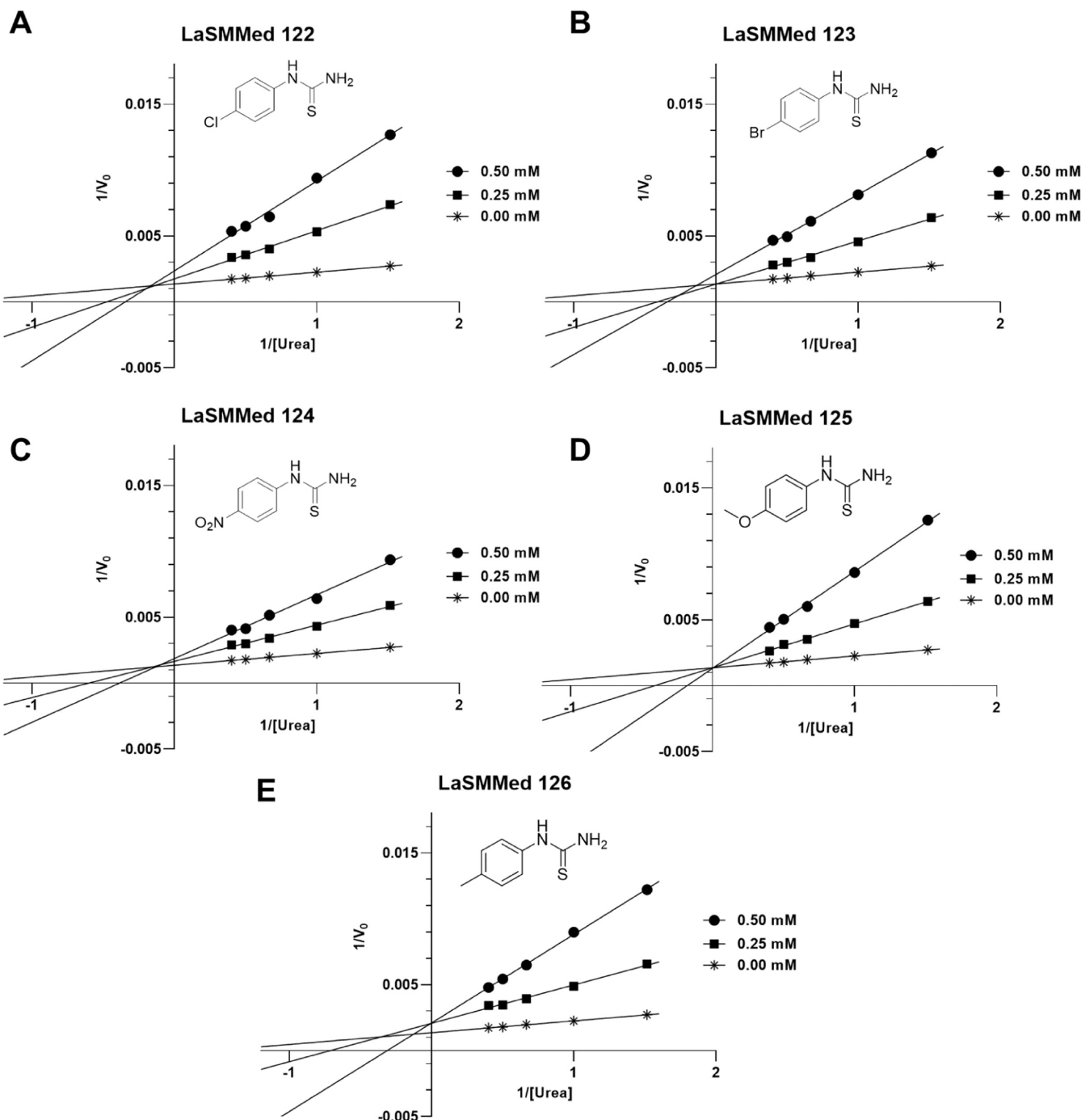


Figure 5. Urease inhibition mode from Lineweaver–Burk plots of the reciprocal reaction rate vs the reciprocal of the substrate (urea) in the absence (*) and in the presence of 0.50 mM (■) and 0.25 mM (●) of compounds LaSMMed 122 (A), LaSMMed 123 (B), LaSMMed 124 (C), LaSMMed 125 (D), and LaSMMed 126 (E).

results showed values significantly greater than 1. This indicates that these inhibitors have a stronger preference for binding to the free enzyme rather than to the enzyme–substrate complex. Consequently, the mixed model tends to resemble competitive inhibition.²⁶

2.6. Molecular Docking and Molecular Dynamics of Arylthioureas LaSMMed 122–126 in CEU. Based on our findings, most inhibitors preferentially form an enzyme–inhibitor complex through a mixed-type mechanism. This process blocks the formation of the urease–urea complex, thereby reducing the enzymatic activity. To further investigate

this, we conducted an *in silico* analysis to explore the interaction between CEU and LaSMMed 122–124 and 126 at the allosteric site. Our goal was to identify the potential interaction characteristics of this class of compounds with the molecular target.

In our previous research, we mapped the structure of CEU, and we identified an allosteric site located in the region referred to as the “hammer handle”, which is at the junction between the $\alpha\beta$ and β domains.²⁵ The molecular docking results of inhibitors LaSMMed 122–124 and 126 indicated

Table 5. Effect of Arylthioureas LaSMMed 122–126 on CEU Kinetic Parameters

LaSMMed	R	K _i (mM)	Alfa (α)	K _m (mM)	V _{max} (μmol min ⁻¹)
LaSMMed 122	Cl	0.089	6.00	0.66	735.50
LaSMMed 123	Br	0.110	9.75	0.67	741.30
LaSMMed 124	NO ₂	0.130	6.13	0.65	733.50
LaSMMed 125	OCH ₃	0.080	-	0.66	737.50
LaSMMed 126	CH ₃	0.100	4.88	0.65	732.30

that they exhibited similar binding poses within this allosteric site of CEU (see Figure 6A).

With the exception of LaSMMed 124 (Figure 6D), all other compounds exhibited hydrogen bonding involving the thiourea subunit with E718 and K716. Specifically, for LaSMMed 122, the NH group interacted with the carboxylate ion of amino acids E718 and K716 at distances of 1.8 and 2.4 Å, respectively (Figure 6B). A similar interaction occurred for LaSMMed 123 at distances of 2.0 Å with E718 and 2.3 Å with K716 (Figure 6C). In the case of LaSMMed 126, the observed hydrogen bond distances were 1.9 and 2.6 Å for the respective amino acids (Figure 6E). Additionally, all three substances demonstrated hydrophobic interactions between the ligands in position 4 of the aromatic ring and the residues Y32 and V36.

LaSMMed 124 showed a hydrogen bond interaction between the NH groups of the thiourea subunit and the carboxylate ion of E742 at distances of 1.8 and 2.2 Å. Additionally, another interaction was observed between the

NO₂ group of the ligand and the amine of K716 at a distance of 2.8 Å (Figure 6D). Weaker hydrophobic interactions were observed between the ligand ring and the alkyl groups of V36 and V744 (Figure 6D).

Regarding molecular docking results to LaSMMed 125 on the active site from the CEU enzyme, we identified hydrogen bond interactions involving the thiourea group and the catalytic amino acids KCX490, A440, and D633, which are critical for Ni²⁺ coordination,³ as well as with G550. Furthermore, hydrophobic interactions were observed with H407, H492, D494, H519, H593, and R606. Notably, the sulfur atom played a key role in the interaction with the Ni²⁺ ion (Figure 7).

We also included an investigation of the competitive inhibitor LaSMMed 125 in our analysis. Our findings indicate that the addition of an oxygen atom, resulting in the formation of a methoxy group (*R* = OCH₃), provides LaSMMed 125 with the active conformation needed to interact with the active site residues, allowing it to function as a competitive inhibitor. In contrast, its derivative, LaSMMed 126 (*R* = CH₃), exhibits mixed-type inhibition.

We investigated the behavior of arylthiourea compounds within an aqueous system at the enzyme's allosteric site. This study employed molecular dynamics simulations on the enzyme with an unoccupied active site (free site). We analyzed the ligand atoms of LaSMMed 122–126 using root-mean-square deviation (RMSD) metrics and found that LaSMMed 123 and LaSMMed 126 were the most stable compounds at the allosteric site. LaSMMed 123 had an RMSD value of 2.03 ± 0.75 Å (Figure 8B), while LaSMMed 126 showed an RMSD

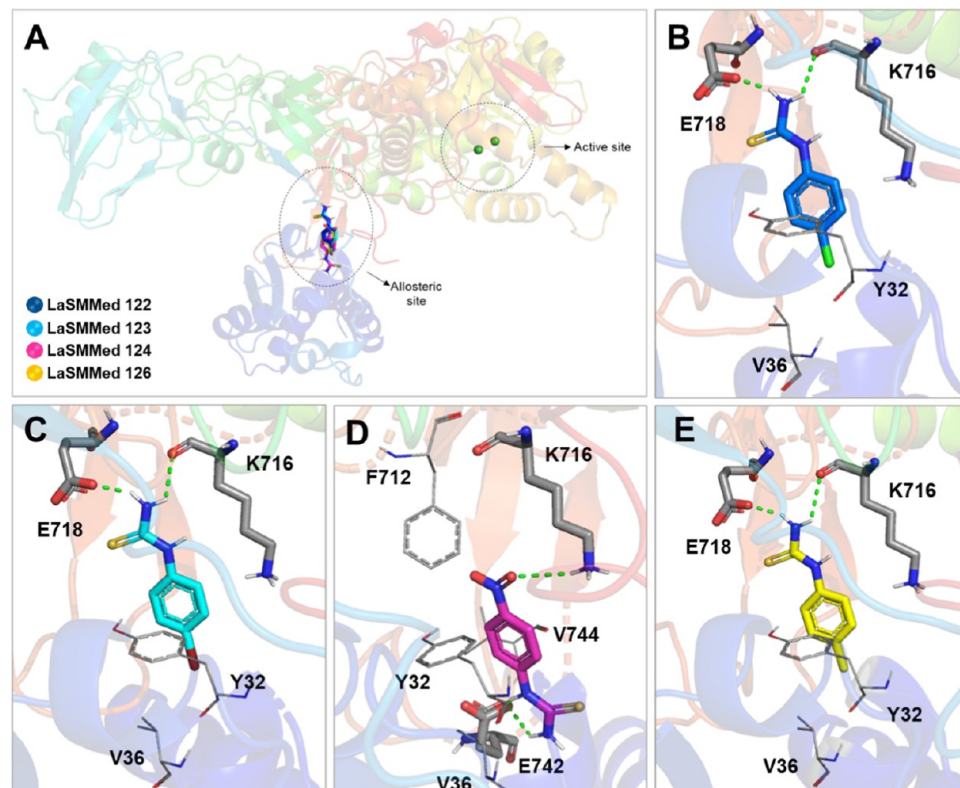


Figure 6. (A) Overlap of inhibitor on the allosteric site from CEU. Interactions of substances (B) LaSMMed 122, (C) 123, (D) 124, and 126 (E) with CEU. The gray sticks represent residues involved in hydrogen bonding, and the lines represent hydrophobic ones. Dashed green lines show hydrogen bonds.

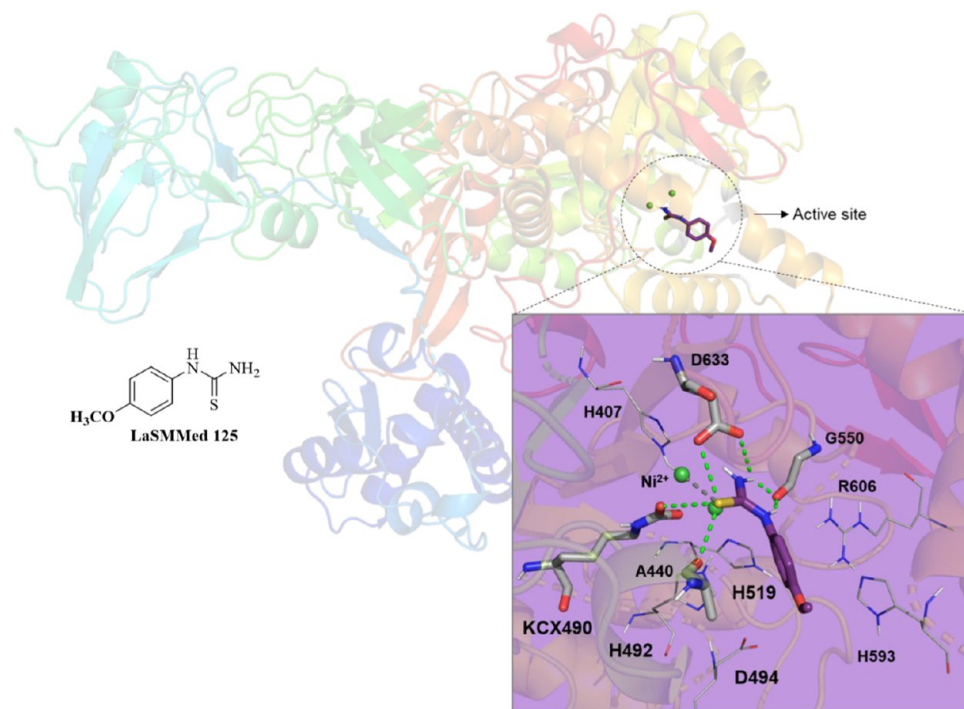


Figure 7. Interactions of the substances LaSMMed 125 on the active site from CEU. The gray sticks represent residues involved in hydrogen bonding, and the lines represent hydrophobic ones. Hydrogen bonds are shown by dashed green lines, and gray dashed lines show metal interaction.

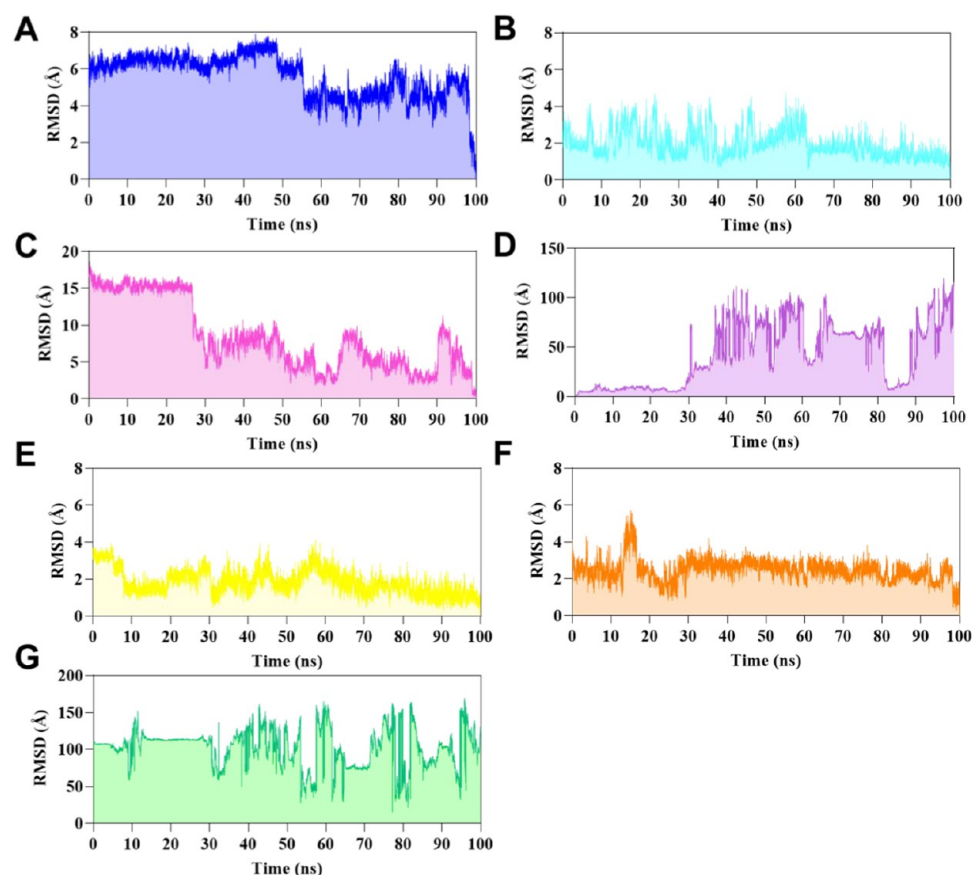


Figure 8. RMSD values during 100 ns of MD simulations based on ligand atoms of (A) LaSMMed 122, (B) 123, (C) 124, (D) 125, (E) 126 (free-site), (F) LaSMMed 126 (occupied-active site with HAE), and (G) HAE (in the presence of LaSMMed 126).

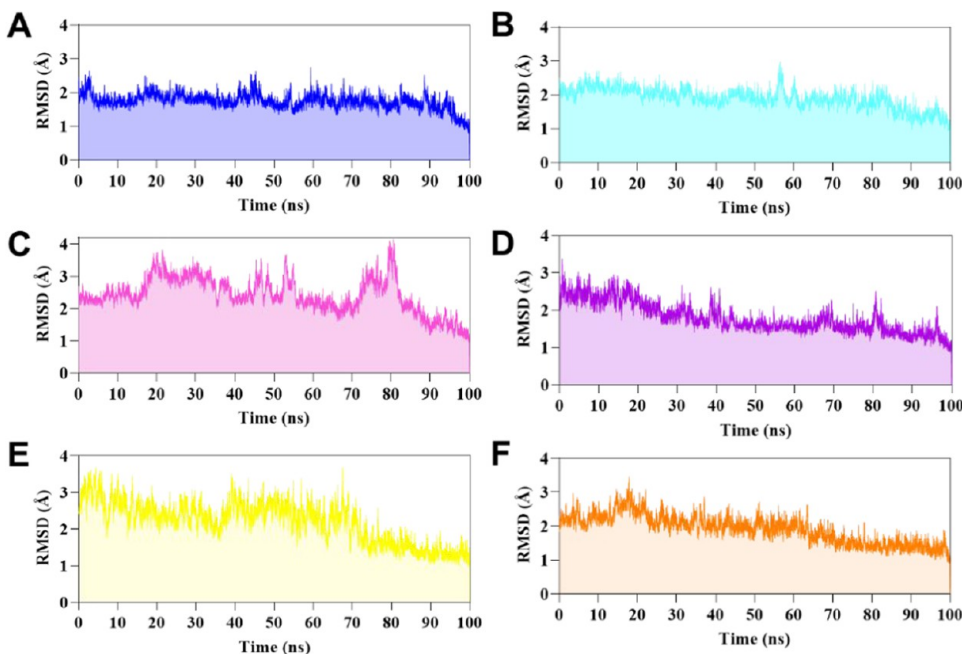


Figure 9. RMSD values during 100 ns of MD simulations based on $\text{C}\alpha$ atoms of protein to LaSMMed (A) 122, (B) 123, (C) 124, (D) 125, (E) 126 (free-site), and (F) LaSMMed 126 (occupied active site with HAE).

value of $2.20 \pm 0.56 \text{ \AA}$ (Figure 8E). In contrast, LaSMMed 122 and LaSMMed 124 had higher RMSD values of 5.58 ± 1.16 and $8.34 \pm 4.67 \text{ \AA}$, respectively. These compounds demonstrated movement in the allosteric site after approximately 50 and 25 ns (Figures 8A,C), compared to their poses, as determined by molecular docking.

CEU has cocrystallized acetohydroxamic acid (HAE), a competitive inhibitor structurally similar to the natural urea substrate. This enables us to simulate its behavior in the presence of inhibitors during molecular dynamics studies, thereby verifying the interaction that may indicate binding to the free enzyme rather than the enzyme–substrate complex in cases of mixed model inhibition.

In this way, we analyzed LaSMMed 126, which exhibited the lowest α value in *in vitro* tests ($\alpha = 4.88$). We investigated this ligand along with inhibitor HAE to simulate the formation of a potential enzyme–substrate-inhibitor complex. During the simulation, LaSMMed 126 remained stable at the allosteric site while HAE occupied the active site, with an RMSD of $2.46 \pm 0.60 \text{ \AA}$ and only a slight variation observed in 15 ns (Figure 8F). As shown in Figure 8G, HAE demonstrated significant variability in its RMSD, with a standard deviation of $102 \pm 26 \text{ \AA}$. Furthermore, during the simulation, HAE disconnected from the complex within the first few nanoseconds (Figure 8G). These findings support the hypothesis that the enzyme–substrate-inhibitor complex does not form in the presence of arylthioureas. Instead, the mixed inhibitors identified in this study preferentially interact with the free enzyme. Finally, we investigated the competitive inhibitor LaSMMed 125 (Figure 8D) within the enzyme’s active site. It demonstrated stability only in the initial 30 ns of the simulation, followed by a brief period between 82 and 90 ns. During this latter phase, high standard deviation values were observed, with a root-mean-square deviation (RMSD) of $42.7 \pm 31.8 \text{ \AA}$. During the 100 ns of MD simulations, the RMSD analysis of $\text{C}\alpha$ atoms from the enzyme exhibited stability ranging from 1.75 to 2.42 \AA (Figure 9A–E). The ligands in the allosteric site showed lower RMSD

values, with LaSMMed 122 at $1.75 \pm 0.23 \text{ \AA}$, LaSMMed 126 (free-site) at $1.86 \pm 0.67 \text{ \AA}$, LaSMMed 126 (occupied-site) at $1.92 \pm 0.42 \text{ \AA}$, and LaSMMed 123 at $1.92 \pm 0.30 \text{ \AA}$. In contrast, LaSMMed 124 had a higher value of $2.42 \pm 0.55 \text{ \AA}$. The RMSD- $\text{C}\alpha$ atoms to LaSMMed 125 at the active site were also low, measuring $1.79 \pm 0.41 \text{ \AA}$ (Figure 9F).

Notably, the root-mean-square-fluctuation (RMSF) calculation of all LaSMMed inhibitors reveals that specific residues exhibit mobility greater than 3.0 \AA for $\text{C}\alpha$ atoms (Figure 10A–F). These residues include Ser41 to Asn131 near the allosteric site (Figure 10G) and Asn580 to Arg609, as well as Pro805 to Lys821 within the active site region (Figure 10G).

The active site region spanning Asn580 to Arg609 exhibited the most significant fluctuations in the presence of ligands LaSMMed 122, 123, 124, and 126 (Figure 10A–C,E). Residue 661, located in the C-terminal domain (Figure 10G) where the active site is located,¹⁹ demonstrated notable RMSF values of 5 and 8 \AA in the presence of ligands LaSMMed 122 and LaSMMed 124, respectively (Figure 10A,C). Additionally, ligand LaSMMed 123 also resulted in RMSF values of approximately 7 \AA for amino acids Pro805-Lys821 within the protein loop (Figure 10B,G).

LaSMMed 126 did not exhibit any significant differences in the RMSF values for residues Asn580–Arg609, whether in the free-enzyme state (Figure 10E) or in the presence of the HAE inhibitor (Figure 10F). However, it showed fluctuation values of less than 3 \AA for residues Ser41–Asn131, which are located near the allosteric site (Figure 10G). In contrast, the presence of competitive inhibitor LaSMMed 125 resulted in values up to 3 \AA for the regions mentioned above (Figure 10D).

In analyzing hydrogen bonds in the allosteric site, LaSMMed 122 formed hydrogen bonds with the residues Tyr32, Lys716, and Glu718 within the first few nanoseconds of simulation (Figure 11A). These interactions persisted throughout the simulation, lasting even after 80 ns, despite a change in the ligand’s orientation. The lifetime of the interactions varied between 6 and 85% (Figure 11A).

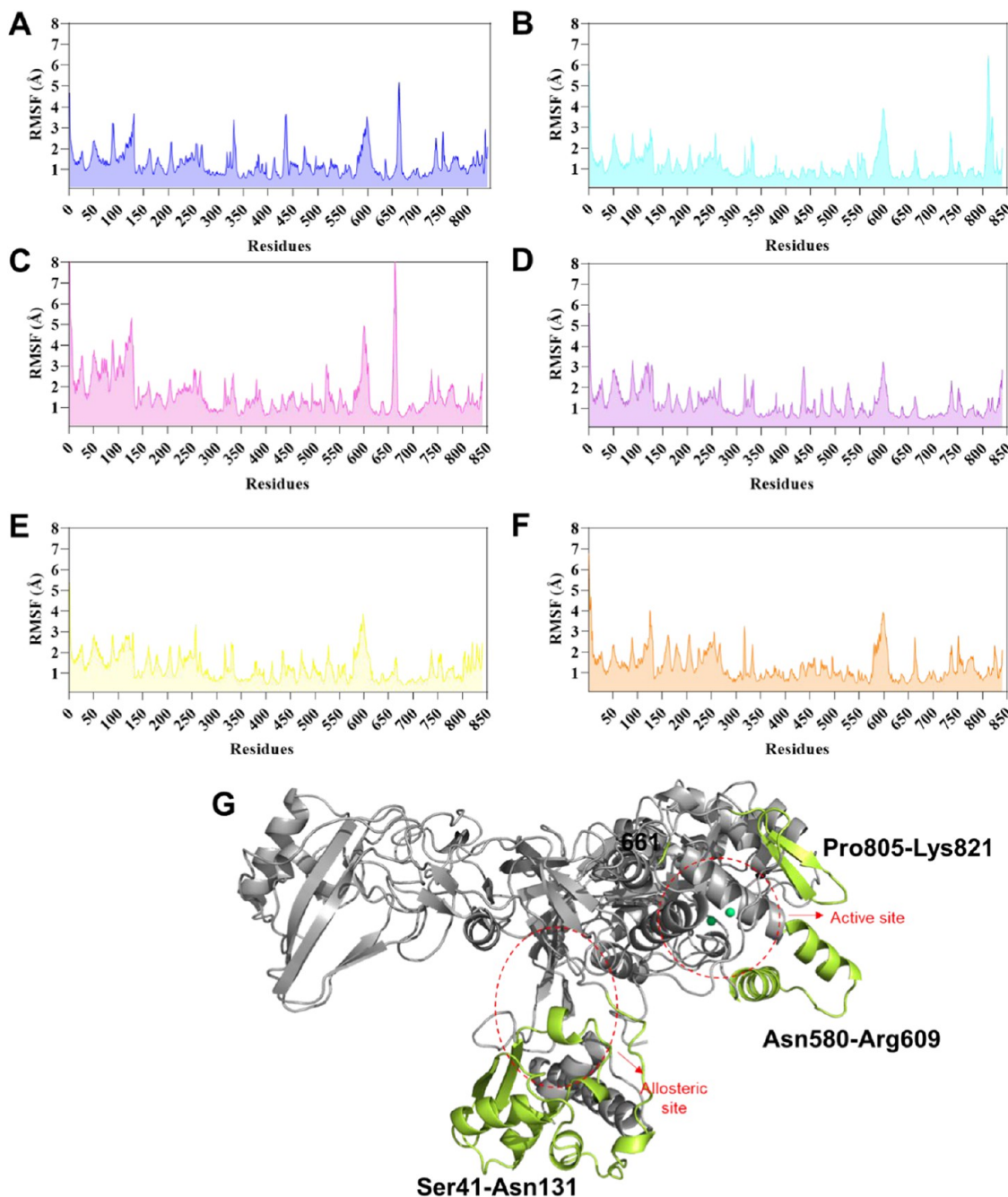


Figure 10. RMSF values during 100 ns of MD simulations based on $C\alpha$ atoms of protein residues to LaSMMed (A) 122, (B) 123, (C) 124, (D) 125, (E) 126 (free-site), and (F) LaSMMed 126 (occupied active site with HAE). (G) CEU 3D structure highlights the residues with the most fluctuations observed in green.

LaSMMed 123 displayed similar interactions to LaSMMed 122, with an H-bond lifetime ranging from 6 to 83% (Figure 11B). These interactions persisted throughout the MD simulation. Additionally, LaSMMed 123 formed another H-bond with Lys-709, likely influenced by the -Br substituent, which is a larger atom (Figure 11B). This interaction positioned the ligand closer to the Tyr32 residue compared with LaSMMed 122, where the bonding occurred between residues Lys716 and Tyr32 (Figure 11A). Furthermore, both compounds did not exhibit significant differences in their poses compared to the molecular docking results (in green, Figure 11A,B), as indicated by the RMSD analyses.

In the H-bond analysis of the allosteric site, LaSMMed 124 initially interacted with Tyr32, Lys709, Asp730, and Lys745 at the start of the simulation. However, there was some movement in its position compared with the docking results (as shown in Figure 12A). After 60 ns, these bonds were lost, and only the interaction with Lys709 remained persistent until the end of the simulation. The lifetimes of these H-bonds varied between 5 and 56.9% (Figure 12A).

Our observations indicated that in the active site, LaSMMed 125 interacted with residues Ala436, Cys592, His593, Gln635, and Ala636 during the first 30 ns of MD simulation (Figure 12B). However, after this initial interaction, the ligand moved out of the active site and only returned between 82 and 90 ns.

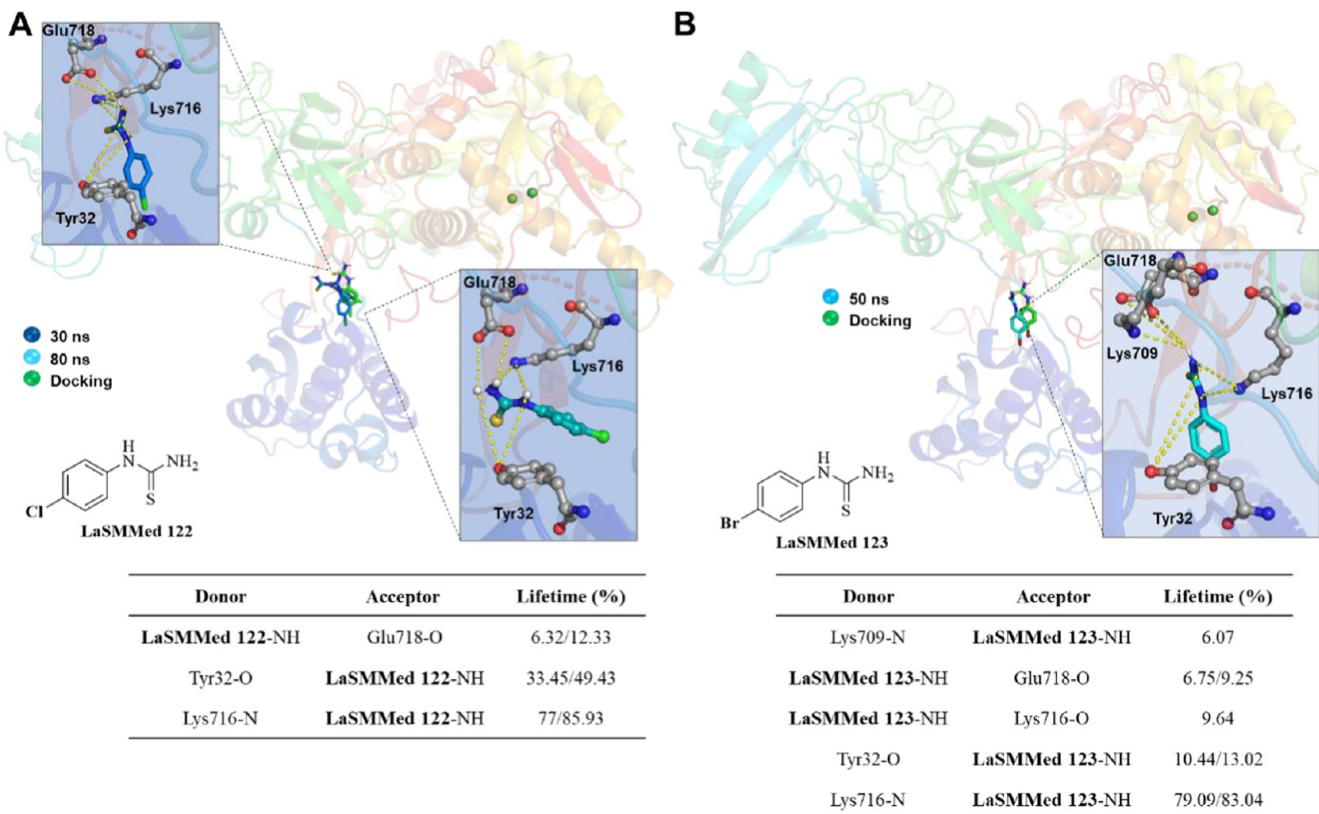


Figure 11. H-bond interactions by molecular dynamics simulations (100 ns) from LaSMMed-CEU complexes. (A) 122; (B) 123. The table shows donor and acceptor groups involved in the H-bonds and their lifetime (%). The ligands involved in H-bond interactions (dashed yellow lines) are displayed in gray sticks and balls. The pose of ligands by docking results is shown in green sticks for comparison.

During this later period, an H-bond with Arg439, located in the outer cavity of the active site, was established, as noted in the RMSD analysis. Although the H-bond interactions of LaSMMed 125 had relatively low lifetimes ranging from 5 to 12% (Figure 12B), they were still sufficient to disrupt the catalytic activity of urease, leading to its inhibition.

In the allosteric site, LaSMMed 126 interacted with Glu718 and Asp730 (21 and 8–74%, respectively) in the enzyme's free state. This interaction formed strong hydrogen bonds that remained stable throughout the simulation. Additionally, the ligand established two other interactions with shorter lifetimes (ranging from 7 to 17%) with Tyr32 and Lys709. Despite a change in orientation, LaSMMed 126 remains bound to the same pocket observed during the docking process (Figure 13A).

In the case of LaSMMed 126, when the enzyme's active site was occupied with HAE, interactions with Glu718 and Asp730 were observed, but these interactions had shorter lifetimes, ranging from 5 to 26%. Furthermore, new hydrogen bonds formed with residues Lys716 and Pro717, with lifetimes between 15 and 28% (Figure 13B). It is important to note that the inhibitor HAE remained in the active site cavity only during the first 15 ns of the simulation (in orange, Figure 13B) when LaSMMed 126 was present in the allosteric. Subsequently, HAE disconnected from the complex, while LaSMMed 126 remained connected to the enzyme without any loss of interaction throughout the process (Figure 13b).

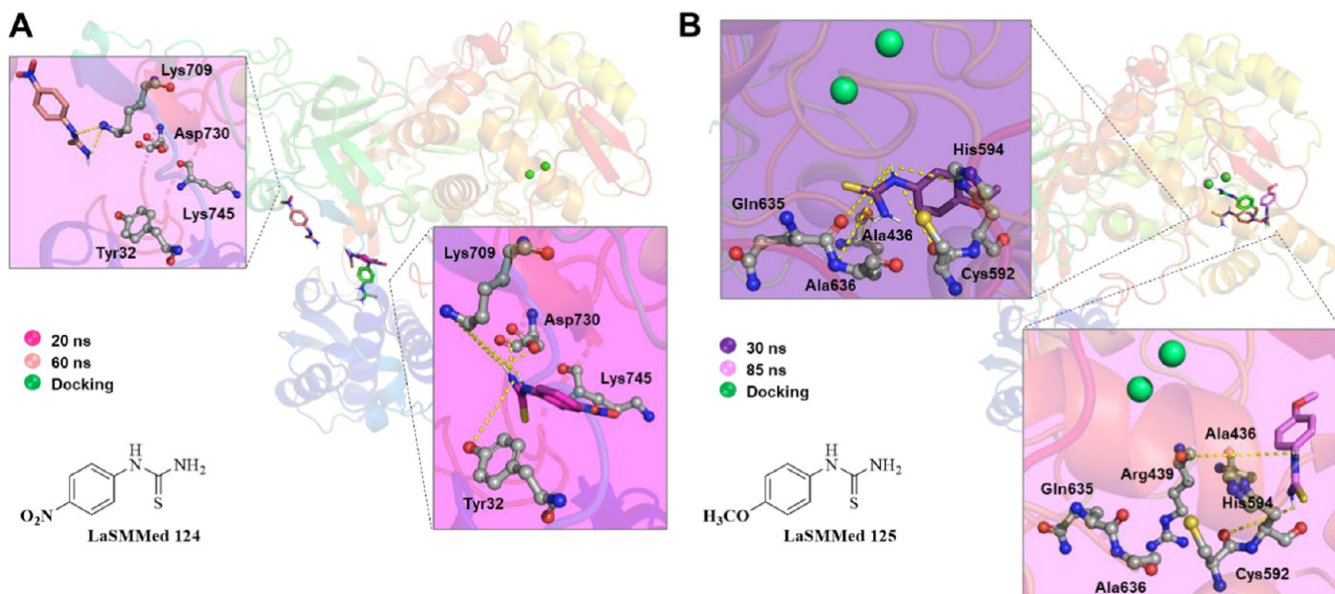
A careful examination of the interaction behavior and lifetime percentages of the arylthiourea-type ligands revealed that they tend to interact with urease in its free state. This

interaction may prevent the formation of an enzyme–substrate complex, mimicking competitive inhibition. Further research could explore the implications of this mechanism and its potential applications in the development of new urease inhibitors.

We calculated the binding free energy (ΔG_{bind}) for the complexes throughout 100 ns of simulation using Linear Interaction Energy (LIE).²⁷ The average interaction energy trajectory results indicate that the LaSMMed-CEU bound state had lower energy than its free state. A similar trend was observed in the electrostatic Coulomb's interactions, suggesting that binding of LaSMMed 122–126 to CEU was favorable.

The binding energy values were consistent with those of the other molecular dynamics analyses. Among the compounds evaluated at the allosteric site, those with the most extended lifetime hydrogen bond interactions exhibited the highest energy binding values. LaSMMed 122 had the highest energy value with a ΔG_{bind} of -18.3 kJ/mol , followed by LaSMMed 123 with $\Delta G_{\text{bind}} = -17.3 \text{ kJ/mol}$. LaSMMed 126 had a $\Delta G_{\text{bind}} = -14.8 \text{ kJ/mol}$ in its free state and a $\Delta G_{\text{bind}} = -15.7 \text{ kJ/mol}$ in its occupied state, while LaSMMed 124 showed a $\Delta G_{\text{bind}} = -12.1 \text{ kJ/mol}$ (Table 6).

In the ligand-bonded state, the derivatives evaluated at the allosteric site (LaSMMed 122, 123, 124, and 126) showed the most significant ΔG_{vwd} values for nonpolar interactions, ranging from -83 to -95 kJ/mol . This can be attributed to the interactions with the Tyr32 residue observed for all of the compounds (Table 6). The most notable contribution to the free energy values came from electrostatic interactions, which



Donor	Acceptor	Lifetime (%)
Tyr32-O	LaSMMed 124-NH	5.32
LaSMMed 124-NH	Lys745-N	5.74
LaSMMed 124-NH	Asp730-O	8.64/9.19
Lys709-N	LaSMMed 124-NH	55.01/56.93

Time	Donor	Acceptor	Lifetime (%)
	LaSMMed 125-NH	Ala436-O	4.77
	LaSMMed 125-NH	His593-N	5.96
0-30 ns	LaSMMed 125-NH	Cys592-O	5.36
	LaSMMed 125-NH	Ala636-N	11.9
	LaSMMed 125-NH	Gln635-O	12.5
82-90 ns	LaSMMed 125-NH	Cys592-O	4.29
	LaSMMed 125-NH	Arg439-O	5.53

Figure 12. H-bond interactions by molecular dynamics simulations (100 ns) from LaSMMed-CEU complexes. (A) LaSMMed 124 (allosteric site); (B) LaSMMed 125 (active site). The table shows donor and acceptor groups involved in the H-bonds and their lifetime (%). The ligands involved in H-bond interactions (dashed yellow lines) are displayed in gray sticks and balls. The poses of ligands by docking results are displayed in green sticks for comparison.

were similar across the four derivatives, ranging from $\Delta G_{el} = -164$ to -187 kJ/mol. Notably, LaSMMed 126, when in the occupied active site state, exhibited an exceptionally high value of $\Delta G_{el} = -337$ kJ/mol (Table 6). Compared with the free state, this energetic value may have been influenced by interactions with the Pro717 residue and the lack of interaction with Tyr32. Additionally, the ligand was closer to the residues of Glu718 and Asp730 than was observed in other cases.

LaSMMed 125 exhibited a low lifetime percentile, resulting in a decreased binding free energy value of $\Delta G_{bind} = -6.9$ kJ/mol. The active site of urease primarily consists of acidic or basic residues, including aspartate, histidine, and arginine.³ Consequently, the most significant contribution to the free energy value for LaSMMed 125 arose from electrostatic interactions, with $\Delta G_{el} = -184.3$ kJ/mol, compared to nonpolar interactions, which contributed $\Delta G_{vwd} = -73.5$ kJ/mol (Table 6).

Additionally, an analysis was performed to evaluate the energetic contributions of residues involved in hydrogen bonds with inhibitors LaSMMed 122–124 and 126 at the allosteric site during molecular dynamics simulations. The residues that most significantly contributed to ΔG_{bind} were Tyr32, Lys716, Glu718, and Asp730 in most cases. Notably, Tyr32 consistently affected the ΔG_{vwd} values across all evaluated complexes. The most substantial energetic contribution came

from the Asp730 residue, with values ranging from -7.36 to -151 kJ/mol, followed by Lys716, which ranged from -14.2 to -80.9 kJ/mol (Table 7).

The analysis of contributions from specific residues supports the finding that in the occupied-site state, LaSMMed 126 shows a greater energetic contribution from residue Pro717 (-8.56) compared to the free state (-3.07 kJ/mol). Conversely, the contribution from Tyr32 decreases significantly from -32.8 kJ/mol in the free state to -7.08 kJ/mol in the occupied state (Table 7). These changes influence the notably high $\Delta G_{el} = -337$ kJ/mol observed for the complex. Furthermore, the contribution of Lys709 to the LaSMMed 124 complex was significantly higher ($\Delta G_{bind} = -56.9$ kJ/mol) than those of the other complexes (Table 7). This finding is further supported by H-bond analysis, which revealed that the interaction with this residue has a longer lifetime of 56.9% in this complex.

The examination of the seven residues in the allosteric site yielded promising findings. The cavity formed by these residues (Figure 14) exhibits hydrophobic characteristics due to the phenyl ring of Tyr32, the pyrrolidine of Pro717, and the carbonic side chain of the lysine residues. This creates an optimal environment for interaction with the phenyl ring from arylthioureas.

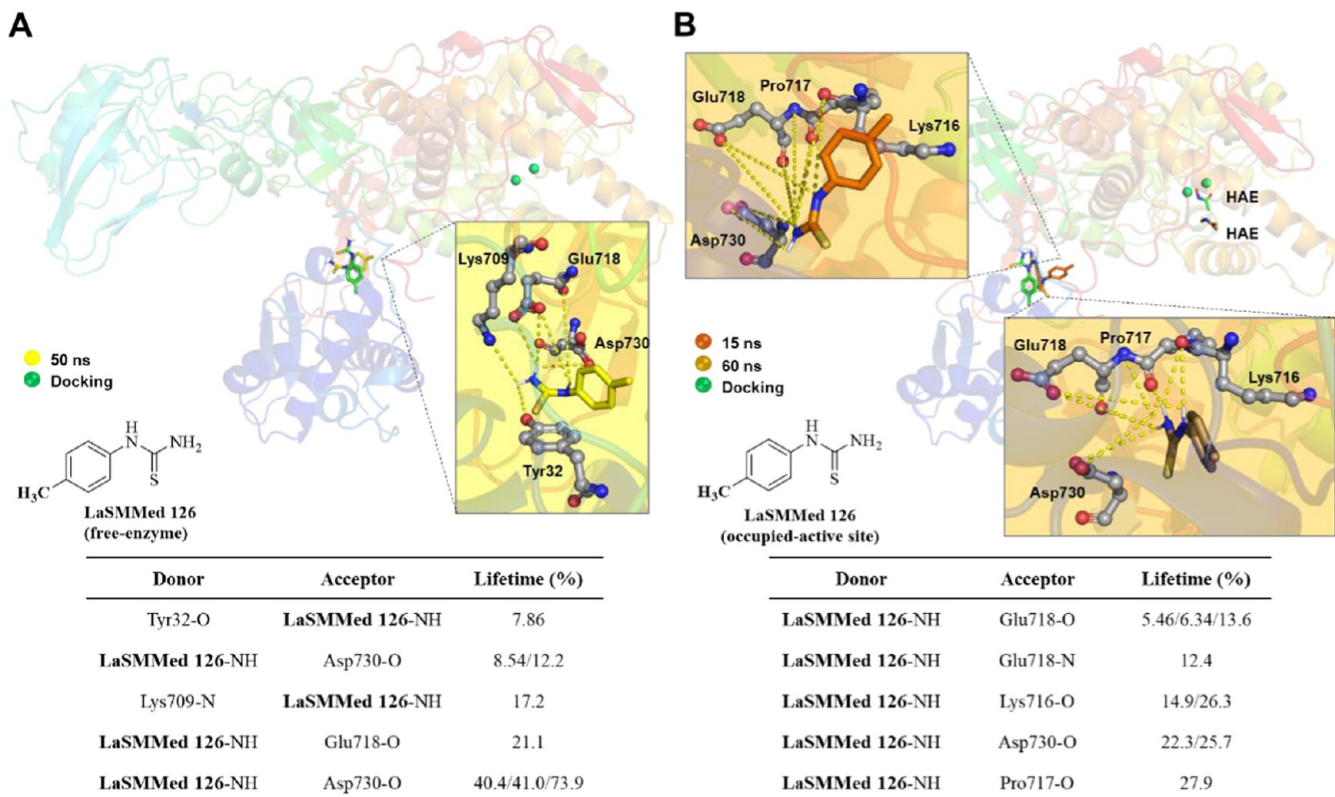


Figure 13. H-bond interactions by molecular dynamics simulations (100 ns) from LaSMMed-CEU complexes. (A) **126** (free-site); (B) **125** (occupied-active site). The table shows donor and acceptor groups involved in the H-bonds and their lifetime (%). The ligands involved in H-bond interactions (dashed yellow lines) are displayed in gray sticks and balls. The pose of ligands by docking results is displayed in green sticks for comparison.

Table 6. Binding Free Energy (ΔG_{bind} Mean \pm Standard Deviation in kJ/mol) of LaSMMed 122-126 Inhibitors on Urease Complexes^a

R	(ΔG^{vdw})bound	(ΔG^{vdw})free	(ΔG^{el})bound	(ΔG^{el})free	ΔG_{bind}	
LaSMMed 122	Cl	-92.9 \pm 0.8	-62.5 \pm 0.4	-164.4 \pm 4.0	-151.3 \pm 0.5	-17.3
LaSMMed 123	Br	-95.0 \pm 0.9	-64.8 \pm 0.4	-172.3 \pm 2.4	-152.4 \pm 1.1	-18.3
LaSMMed 124	NO ₂	-89.9 \pm 3.3	-70.6 \pm 0.2	-176.7 \pm 7.6	-161.6 \pm 0.3	-12.1
LaSMMed 125	OCH ₃	-73.5 \pm 3.3	-64.0 \pm 0.3	-184.3 \pm 6.2	-171.0 \pm 0.9	-6.9
LaSMMed 126^f	CH ₃	-68.6 \pm 1.2	-42.3 \pm 0.5	-347.5 \pm 6.5	-337.1 \pm 1.9	-14.8
LaSMMed 126^o	CH ₃	-83.2 \pm 0.5	-63.7 \pm 0.3	-187.1 \pm 2.7	-149.7 \pm 0.7	-15.7

^af = free state, o = occupied active site. The vdw refers to nonpolar interactions modeled by a Lennard-Jones potential, and el denotes electrostatic interactions by Coulomb potential; standard coefficients $\alpha = 0.161$ and $\beta = 0.50$.

Table 7. Binding Free Energy of Amino Acids in Interaction with LaSMMed 122-126 Inhibitors on Urease Complexes^a

residues	LaSMMed 122	LaSMMed 123	LaSMMed 124	LaSMMed 126 ^b	LaSMMed 126 ^c
Tyr32	-8.77	-18.0	-9.03	-32.8	-7.08
Lys709	-4.20	-0.18	-56.9	-0.15	-0.27
Lys716	-51.9	-80.9	-2.95	-21.6	-14.2
Pro717	-1.51	-1.40	-0.24	-3.07	-8.56
Glu718	-9.30	-8.33	-3.22	-24.8	-9.28
Asp730	-25.5	-20.4	-7.36	-151	-12.5
Lys745	-1.48	-1.89	-0.96	-2.89	-2.85

^aIn bold, the higher values of ΔG_{bind} to residues by complex. ^bFree state. ^cOccupied active site.

Furthermore, the charged amino groups of lysine and carboxyl groups of aspartate and glutamate provide excellent

conditions for H-bond interactions with the thiourea groups of the derivatives. Collectively, these features form a criteria

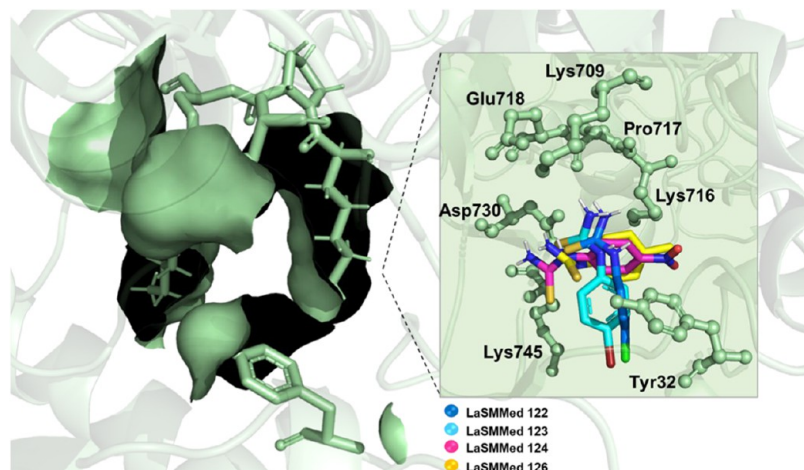


Figure 14. Allosteric site cavity formed by residues Tyr32, Lys709, Lys716, Pro717, Glu718, Asp730, and Lys745 to interactions with LaSMMed 122–124 and LaSMMed 126.

binding pocket that is highly suitable for complexing these derivatives with the urease (Figure 14).

3. CONCLUSIONS

In summary, six thiourea derivatives derived from cinnamic acid (LaSMMed 37–46) were identified through virtual screening as potential urease inhibitors. These compounds interacted with key residues in the active site of HPU, including Ni^{2+} ions and histidine residues, which are crucial for enzymatic activity. The most promising compound, LaSMMed 42, showed an inhibition rate against CEU, comparable to that of the standard thiourea. A new series of arylthioureas (LaSMMed 122–126) was designed and synthesized based on the structure of LaSMMed 42. These compounds exhibited a strong urease inhibitory activity. The arylthioureas demonstrated mixed or competitive inhibition mechanisms. The nitro-substituted derivative, LaSMMed 124, showed the highest inhibitory potency.

Molecular dynamics simulations revealed that the arylthioureas preferentially bind to the allosteric site of CEU, forming stable interactions with key residues, such as Tyr32, Lys716, and Glu718. These interactions were consistent with the mixed inhibition mechanism observed *in vitro*. The competitive inhibitor LaSMMed 125 interacted with the active site residues, including Ni^{2+} ions, while the other arylthioureas showed mixed inhibition by binding to the allosteric site. The primary thiourea subunit was essential for binding to the enzyme's active site, particularly interacting with Ni^{2+} ions and key amino acid residues. The presence of electron-donating or -withdrawing groups on the aryl ring influenced the inhibitory potency, with the nitro group (LaSMMed 124) providing the highest activity. Future studies might investigate further structural modifications, such as adding substituents at positions 2 and 3 of arylthioureas, to enhance the potency of these compounds.

The study successfully identified a series of thiourea and arylthiourea derivatives as potent urease inhibitors. The most effective compounds, particularly LaSMMed 42 and arylthioureas LaSMMed 122–126, showed promising inhibitory activity against urease. The molecular docking and dynamics simulations provided insights into the binding mechanisms and structural requirements for effective urease inhibition, support-

ing the potential development of these compounds as novel therapeutic agents against urease-producing pathogens.

4. EXPERIMENTAL SECTION

4.1. General. Analytical-grade solvents were used as received. For synthetic purposes, solvents and reagents underwent meticulous treatment, distillation, and drying, tailored to the specific requirements outlined in the adopted methodologies and adhering to the procedures elucidated by Armarego and Chai (2003).²⁸ NMR spectra were obtained

on a Bruker spectrometer (Model Ascend 400) operating at 400.13 MHz for ^1H and 100.13 MHz for ^{13}C equipped with a 5 mm broadband probe. Deuterated solvents, such as chloroform (CDCl_3 , 7.26 ppm) or dimethyl sulfoxide ($\text{DMSO}-d_6$, 2.50 ppm), were employed for recording the spectra. Signal multiplicities were denoted as singlet (*s*), doublet (*d*), triplet (*t*), quartet (*q*), double doublet (*dd*), double double–doublet (*ddd*), and multiplet (*m*), while coupling constants (*J*) were expressed in Hz. The spectroscopic data for the synthesized substances are detailed in the Supporting Information.

4.2. Synthesis of Arylthioureas and Cinnamic Acid Derivatives in the LaSMMed Chemical Library.

4.2.1. General Procedure for the Synthesis of Cinnamic Acid Derivatives (LaSMMed 37–45). Cinnamic acid derivatives were synthesized using the methodology outlined by Brito et al. (2015), with pertinent modifications.²¹ In a 500 mL round-bottom flask, a solution of cinnamic acid (100 mmol) dissolved in 250 mL of dichloromethane, 1.0 mL of dimethylformamide, and 125 mmol of SOCl_2 was combined. The reaction mixture was then refluxed and stirred for 3 h. Subsequently, the solvent was evaporated under reduced pressure, yielding cinnamoyl chloride as an orange solid product. In the same reaction flask employed for chloride formation, 200 mL of dried acetone was added, along with 100 mmol of NH_4SCN (1.0 equiv concerning cinnamic acid). The reaction continued under stirring and reflux for 15 min, resulting in the *in situ* formation of cinnamoyl thiocyanate. A 10 mL aliquot of the obtained thiocyanate was dissolved in 10 mL of dry acetone, and with stirring at room temperature, the corresponding amine (10 mmol, 1.0 equiv) was gradually introduced to form the LaSMMed 37–46 derivatives. The reaction mixture was stirred at room temperature for

approximately 40 min. Afterward, the reaction mixture was poured onto crushed ice, and the resulting precipitate was filtered under vacuum. LaSMMed 37–46 were obtained in yields ranging from 62 to 90% after recrystallization in ethanol.

4.2.2. General Procedure for the Synthesis of Arylthioureas (LaSMMed 122–126). The synthesis of arylthioureas (LaSMMed 122–126) adhered to the procedure outlined by Kataria and collaborators with specific modifications.²⁹ A 25 mL round-bottom flask was charged with the corresponding aniline (16 mmol, 1.0 equiv). To this, 5 mL of concentrated hydrochloric acid was gradually added while continuously stirring at room temperature. The reaction was allowed to proceed under these conditions for approximately 5 to 10 min until a visible change occurred in the reaction medium. At this point, a solution of ammonium thiocyanate (1.5 equiv), previously dissolved in 6 mL of distilled water, was added to the flask. The reaction mixture was stirred at room temperature for an additional 15 min until a noticeable change occurred. After this period, the mixture was heated to a temperature between 70 and 80 °C. Within approximately 30 min, the solid in the medium dissolved, and after several more hours, a color change was observed. Finally, the reaction mixture was then stirred and heated for an additional 24 to 26 h. Afterward, the reaction mixture was poured onto crushed ice, and the resulting precipitate was filtered under vacuum. The products were purified by washing with methanol (2 × 10 mL), resulting in arylthioureas LaSMMed 122–126 with yields ranging from 38 to 48%.

4.3. Molecular Modeling. **4.3.1. Preparation of Three-Dimensional Structures of Urease.** Crystallographic structures of ureases from *C. ensiformis* and *H. pylori*, identified by the respective PDB codes 4H9M and 6ZJA, were obtained from the RSCB Protein Data Bank. These structures, featuring resolutions of 1.52 and 2.00 Å, included cocrystallized ligands: acetohydroxamic acid (HAE) for CEU and the inhibitor 2-[1-(3,5-dimethylphenyl)-1H-imidazol-2-yl]sulfanyl]-N-hydroxyacetamide (DJM) for HPU. Before the virtual screening, these structures were processed in Discovery Studio Visualizer software (v.21.1.0.20298). In the case of CEU, water (HOH) and 1,2-ethanediol (EDO) molecules were removed, while for HPU, water molecules and noncontributing tertiary chains were excluded. The quaternary structure of the enzyme was further reduced to five chains (A, B, Q, N, and R) to optimize computational efficiency.

4.3.2. Preparation of Ligands. The three-dimensional structures of the molecules were constructed using Discovery Studio Visualizer (v.19.1.0.18287)³⁰ and subjected to preliminary energy minimization by molecular mechanics (MMFF) through the “Clean Geometry” command. The protonation state of structures at pH 7.4 was verified using MarvinSketch (v.19.21.0), and most species charges were applied to the correct structures from Discovery Studio Visualizer. For additional structural optimization, ligands underwent energy minimization by the semiempirical method PM7, utilizing the MOPAC2016 program through the Mercury program interface (2020.2.0). All substances from the LaSMMed chemical library used in the virtual screening process are listed in *Supporting Information*.

4.3.3. Molecular Docking. **4.3.3.1. Helicobacter pylori.** The three-dimensional structure of urease, obtained through electron microscopy, was prepared for GOLD Suite program calculations (v. 2021.3.0).³¹ Like CEU, the structure was

adjusted by removing the cocrystallized ligand and adding hydrogen atoms.

The center of the active site radius was determined as the midpoint between the nickel atoms [Ni(601) and Ni(602)], with coordinates of X = 225.1450, Y = 246.0130, and Z = 196.5110, and a radius of 15 Å. Molecular docking of the ligand was carried out in flexible mode for the ligand and rigid mode for the protein, generating 50 docking poses for DJM. The four scoring functions available in the GOLD program (GoldScore, ChemScore, CHEMPLP, and ASP) were employed, utilizing default program settings for calculations.

The docking methodology applied to the ligands was validated through redocking using the ASP scoring function, 50 docking poses, a radius of 15 Å, and the midpoint between the Ni ions as the center. Interactions were analyzed using Discovery Studio Visualizer (v.21.1.0.20298), and figures were generated with Pymol (v2.0.4).³² After validation, the same parameters were applied to ligands from the LaSMMed chemical library.

4.3.3.2. Canavalia ensiformis. The molecular modeling study was conducted using the GOLD Suite program (v.2020.1.0, with subsequent studies using v.2022.2.0). The crystallographic structure of urease was prepared for calculations within the software interface by eliminating the cocrystallized ligand and adding hydrogen atoms.

To molecular docking in the active site was applied ligand LaSMMed 125, the center of the radius was defined as the midpoint between the nickel atoms [Ni(901) and Ni(902)], with coordinates X = 18.7825, Y = -57.8095, and Z = -24.1515.¹⁸ For cocrystallized acetohydroxamic acid (HAE), 50 docking poses were generated using the four scoring functions available (GoldScore, ChemScore, CHEMPLP, and ASP), employing default program settings for calculations, considering the one with lower root mean square deviation (RMSD) <2.00 Å to the protocol. The methodology was then validated by redocking HAE, using the ASP scoring function, 50 docking poses, a radius of 15 Å, and the midpoint between the Ni ions as the center.

The molecular docking of compounds LaSMMed 122, 123, 124, and 126 in the allosteric site was defined by coordinates x: 61.8344, y: 23.2354, and z: 89.2500 after the FTMap server analysis (<https://ftmap.bu.edu/>) reported in our previous work²⁵ using the ASP scoring function, 50 docking poses, and a radius of 13 Å. Ligands LaSMMed 122, 123, and 124 were docked in the allosteric site without the inhibitor hydroxamic acid (HAE) on the active site (free-site). In contrast, LaSMMed 126 was docked in the allosteric site with HAE within (occupied site) and out of the active site.

Molecular docking was conducted in the rigid mode for the protein and the flexible mode for the ligands. The ligand–protein complexes were analyzed by examining interactions using the Discovery Studio Visualizer program (v.19.1.0.18287). Figures were generated using the Pymol program (1.7.4.5 Edu).³²

4.3.4. Molecular Dynamics. The poses obtained in the CEU docking studies in the active or allosteric sites were used for molecular dynamics simulations with the CHARMM36 force field³³ employing the GROMACS 2021 program³⁴ following the protocol established by our research group.¹⁸ The protonation state was determined for CEU, considering the pH of 7.4 determined using the H⁺ server.³⁵ Each protein–ligand system was inserted and centered in a triclinic box (dimensions: 13.072 × 9.617 × 8.975 nm; volume:

1128.25 nm³) with periodic conditions. The water model considered was TIP3P,³⁶ and the complex (target–ligand–water) was neutralized with 19 atoms of Na⁺ ions. Ligand parameters were retrieved from the CGenFF server by uploading the mol2 files with the server's default settings, and these parameters were incorporated into the protein chain. We obtained the str format from these data, and a script was used to generate the itp and prm files, which are crucial for establishing the topology of the ligands.³⁷ The energy minimization, equilibration, and production steps were executed according to our previous work.^{18,38} The energy minimization process was achieved first with the steepest-descent algorithm and then with the gradient conjugate algorithm, applying convergence criteria of 1000 and 100 kJ mol⁻¹.nm⁻¹, respectively. Next, the equilibration step was performed at 300 K and 1 bar with positional restraints applied to the entire system, except for ions and water molecules. In the first step (1 ns), the NVT ensemble was kept constant, and in the second step (1 ns), the system was considered as an isothermal–isobaric (NPT) ensemble. This equilibration enables atomic speeds that align with the target temperature and pressure. Constraining the protein–ligand atoms also helps ions and water molecules optimally organize along the protein's surface, creating structured solvation layers. Temperature control was achieved with the V-rescale thermostat³⁹ and pressure control through the Parrinello–Rahman barostat.⁴⁰ All bonds to hydrogen atoms in the complex were constrained using the linear constrained solver (LINCS) algorithm.⁴¹ The long-distance electrostatic interactions were treated using the Particle-Mesh Ewald (PME) algorithm,⁴² and the cutoff radius applied to the van der Waals and Coulomb interactions was 1 nm. Following equilibration, production MD simulations were performed for 100 ns within the NPT ensemble, applying no positional restraints, with a 2 fs integration time and a cutoff radius of 10 Å for long-distance interactions. All complexes were evaluated regarding RMSD (gmx_rms), RMSF (gmx_rmsf), and hydrogen bonds (gmx_hbond) with a cutoff radius of 5.0 Å and a cutoff angle of 30 Å, applying the GROMACS 2021 modules. The HbMap2Grace software⁴³ was used to calculate the frequency of the hydrogen bonds, and the VMD software⁴⁴ was used to visualize the trajectories of the simulations. The binding free energies (ΔG_{bind}) for 100 ns of molecular simulations were calculated using the Linear Interaction Energy (LIE) method with standard coefficients $\alpha = 0.161$ and $\beta = 0.50$ ²⁷ through the module added to GROMACS 5.1.4.⁴⁵ We conducted a conformational cluster analysis using the gmx_cluster module from GROMACS 2021 to select 20 thermodynamically appropriate 20 frames for binding free energy calculations. The reference configuration was chosen from the most populated cluster, which reflects the structurally dominant conformation.

4.4. Enzyme Assays. **4.4.1. Enzyme Inhibition of Urease from *C. ensiformis*.** The *in vitro* inhibitory activity of *C. ensiformis* urease was conducted using the indophenol reaction, also known as the Berthlot Reaction.⁴⁶ Commercially purchased urease from Merck (Sigma-Aldrich), Jack bean type III (CAS 9002–13–5), was utilized, and the methodology was adapted from Khan et al. (2017).

The assays were performed in triplicate on a 96-well plate, as described by our research group.^{18,19} The procedure involved adding 100 μL of urea (10 mM), 55.0 μL of sodium phosphate buffer solution (100 mM, pH 7.4) supplemented with EDTA (1 mM), and 10 μL of the test substance at 2.00 mM for

inhibition percentage assays, previously dissolved in methanol. Subsequently, 25.0 μL of urease enzyme solution (0.0035 mM) was added, and the reaction mixture was incubated at 45–50 °C for 30 min. After incubation, 40.0 μL of phenol reagent (1% phenol and 0.05% sodium nitroprusside) and 40.0 μL of alkaline reagent (1.0% NaOH and 0.05% sodium nitroprusside) were added.⁴⁷ The reaction rested for 15 min, and the absorbance was read at 630 nm using a Loccus model LMR-96i UV-visible microplate reader.

The inhibition percentage (%I) was calculated using the following formula:

$$\%I = 100 - \left(\frac{\text{Abs}_{\text{sample}}}{\text{Abs}_{\text{control}}} \times 100 \right)$$

Abs_{sample} is the absorbance observed for the samples, and Abs_{control} is the absorbance observed for the positive control. Thiourea (2.00 mM) served as the standard inhibitor.

To determine half of the maximum inhibitory concentration (IC₅₀), substances LaSMMed 42, LaSMMed 122–126, and the thiourea control were tested at different concentrations (0.2, 0.4, 0.8, 1.0, 1.4, and 2.0 mM). The IC₅₀ values were calculated using GraphPad Prism 8.0.2, employing a dose-response curve.

4.4.2. Enzyme Kinetics. Enzyme kinetics were studied following previous work by our research group.^{18,19} The same reaction mixture was applied to determine inhibitory activity, and the IC₅₀ was adopted to study enzyme kinetics in *C. ensiformis* urease. However, only two concentrations of the test substance were used (0.50 and 0.25 mM), along with five different concentrations of urea substrate (0.66, 1.00, 1.50, 2.00, and 2.50 mM) for each sample. The absorbance of the reaction mixture was recorded at 630 nm using a Loccus model LMR-96i UV-visible microplate reader. Michaelis–Menten (nonlinear regression) and Lineweaver–Burk (linear regression) plots, as well as the determination of inhibition constants (K_i), K_m , α , and V_{max} were made using GraphPad Prism software (version 8.0.2). Enzymatic activity was calculated using an ammonium chloride calibration curve. One unit of enzymatic activity (U) is the amount of enzyme capable of releasing 1 μmol of ammonia per minute of reaction ($U = 1 \mu\text{mol NH}_4^+ \text{ min}^{-1} \mu\text{mol enzyme}^{-1}$). The assays were performed in triplicate.

4.5. Statistical Analysis. Statistical analyses were conducted using the SISVAR program (version 5.8).⁴⁸ Different letters indicate a significant difference between treatments using the Scott–Knott test ($P < 0.05$).

■ ASSOCIATED CONTENT

● Supporting Information

The Supporting Information is available free of charge at <https://pubs.acs.org/doi/10.1021/acsomega.Sc01648>.

Identifier of the compounds from LaSMMed chemical library; Interactions observed in the molecular docking with HPU; NMR spectra of the synthesized substances (PDF)

■ AUTHOR INFORMATION

Corresponding Author

Marcelle L. F. Bispo – Laboratório de Síntese de Moléculas Medicinais (LaSMMed), Departamento de Química, Universidade Estadual de Londrina (UEL), Londrina,

Paraná 86057-970, Brasil;  orcid.org/0000-0002-6001-360X; Email: mlfbispo@uel.br

Authors

Marcíeli Fabris – Laboratório de Síntese de Moléculas Medicinais (LaSMMed), Departamento de Química, Universidade Estadual de Londrina (UEL), Londrina, Paraná 86057-970, Brasil

Priscila G. Camargo – Faculdade de Farmácia, Departamento de Fármacos e Medicamentos, Universidade Federal do Rio de Janeiro, Rio de Janeiro, Rio de Janeiro 21941-170, Brasil

Mariana L. Silva – Laboratório de Síntese de Moléculas Medicinais (LaSMMed), Departamento de Química, Universidade Estadual de Londrina (UEL), Londrina, Paraná 86057-970, Brasil

Camilo H. S. Lima – Laboratório de Modelagem Molecular (LabMMol), Instituto de Química, Universidade Federal do Rio de Janeiro, Rio de Janeiro, Rio de Janeiro 21941-909, Brasil;  orcid.org/0000-0002-5579-7809

Magaly G. Albuquerque – Laboratório de Modelagem Molecular (LabMMol), Instituto de Química, Universidade Federal do Rio de Janeiro, Rio de Janeiro, Rio de Janeiro 21941-909, Brasil

Carlos R. Rodrigues – Faculdade de Farmácia, Departamento de Fármacos e Medicamentos, Universidade Federal do Rio de Janeiro, Rio de Janeiro, Rio de Janeiro 21941-170, Brasil

Nilton M. Nascimento-Júnior – Laboratório de Química Medicinal, Síntese Orgânica e Modelagem Molecular (LaQMedSOMM), Departamento de Química e Bioquímica, Instituto de Química, Universidade Estadual Paulista (UNESP), Araraquara, São Paulo 14800-060, Brasil;  orcid.org/0000-0002-1543-419X

Complete contact information is available at:
<https://pubs.acs.org/10.1021/acsomega.5c01648>

Funding

The Article Processing Charge for the publication of this research was funded by the Coordenacão de Aperfeiçoamento de Pessoal de Nível Superior (CAPES), Brazil (ROR identifier: 00x0ma614).

Notes

The authors declare no competing financial interest.

ACKNOWLEDGMENTS

This work was made possible, partly, by the National Institute of Science and Technology (INCT) on Urease Inhibitors of Agricultural and Medicinal Interest and the Network of Biostimulants and Increased Efficiency Fertilizers (CNPq; Grant # 406744/2022-0, FAPEMIG Grants # RED-00082-23 and APQ-02103-23, and CAPES Grants # 88887.954439/2024-00). The authors are grateful to Coordenação de Aperfeiçoamento de Pessoal de Nível Superior (CAPES, Financial Code 01) and Fundação de Amparo à Pesquisa do Estado do Rio de Janeiro (FAPERJ, SEI-260003/019723/2022, SEI-260003/003788/2022, and SEI-260003/00692/2023) for the financial support and scholarship.

REFERENCES

- (1) Krajewska, B. Ureases I. Functional, Catalytic and Kinetic Properties: A Review. *J. Mol. Catal. B Enzym.* **2009**, *59* (1–3), 9–21.
- (2) Lippard, S. At Last—the Crystal Structure of Urease. *Science* **80(-)** *1995*, *268* (5213), 996–997.
- (3) Fabris, M.; Nascimento-júnior, N. M.; Bispo, M. L. F.; Camargo, P. G. Computational Strategies Targeting Inhibition of *Helicobacter pylori* and *Cryptococcus neoformans* Ureases. *Curr. Pharm. Des.* **2023**, *29*, 777–792, DOI: 10.2174/1381612829666230329122902.
- (4) Alexander, S. M.; Retnakumar, R. J.; Chouhan, D.; Devi, T. N. B.; Dharmaseelan, S.; Devadas, K.; Thapa, N.; Tamang, J. P.; Lamtha, S. C.; Chattopadhyay, S. *Helicobacter Pylori* in Human Stomach: The Inconsistencies in Clinical Outcomes and the Probable Causes. *Front. Microbiol.* **2021**, *12*, No. 713955, DOI: 10.3389/fmicb.2021.713955.
- (5) Yuan, C.; Adeloye, D.; Luk, T. T.; Huang, L.; He, Y.; Xu, Y.; Ye, X.; Yi, Q.; Song, P.; Rudan, I. The Global Prevalence of and Factors Associated with *Helicobacter Pylori* Infection in Children: A Systematic Review and Meta-Analysis. *Lancet Child Adolesc. Heal.* **2022**, *6* (3), 185–194.
- (6) Sung, H.; Ferlay, J.; Siegel, R. L.; Laversanne, M.; Soerjomataram, I.; Jemal, A.; Bray, F. Global Cancer Statistics 2020: GLOBOCAN Estimates of Incidence and Mortality Worldwide for 36 Cancers in 185 Countries. *CA. Cancer J. Clin.* **2021**, *71* (3), 209–249.
- (7) de Martel, C.; Georges, D.; Bray, F.; Ferlay, J.; Clifford, G. M. Global Burden of Cancer Attributable to Infections in 2018: A Worldwide Incidence Analysis. *Lancet Glob. Heal.* **2020**, *8* (2), e180–e190.
- (8) de Carvalho, P. G. C.; Ribeiro, J. M.; Nakazato, G.; Garbin, R. P. B.; Ogatta, S. F. Y.; de Fátima, Â.; Bispo, M. L. F.; Macedo, F., Jr Synthesis and Antimicrobial Activity of Thiohydantoins Derived from L-Amino Acids. *Lett. Drug Des. Discovery* **2020**, *17*, 94–102, DOI: 10.2174/157018081666181212153011.
- (9) Brito, T. O.; Abreu, L. O.; Gomes, K. M.; Lourenço, M. C. S.; Pereira, P. M. L.; Yamada-Ogatta, S. F.; de Fátima, Â.; Tisher, C. A.; M, F., Jr; Bispo, M. L. F. Benzoylthioureas: Design, Synthesis and Antimycobacterial Evaluation. *Med. Chem. (Los Angeles)* **2018**, *16* (1), 93–103.
- (10) Fagundes, T. R.; Bortoleti, B.; Camargo, P.; Concato, V.; Tomiotti-Pellissier, F.; Carloto, A.; Panis, C.; Bispo, M.; Junior, F. M.; Conchon-Costa, I.; Pavanelli, W. Patterns of Cell Death Induced by Thiohydantoins in Human MCF-7 Breast Cancer Cells. *Anticancer Agents Med. Chem.* **2022**, *22*, No. 1592.
- (11) de Santiago-Silva, K. M.; da Silva Bortoleti, B. T.; de Oliveira Brito, T.; Costa, I. C.; da Silva Lima, C. H.; Macedo, F., Jr; Miranda-Sapla, M. M.; Pavanelli, W. R.; de Lima Ferreira Bispo, M. Exploring the Antileishmanial Activity of *N^{1,N²}*-Disubstituted-Benzoylguanidines: Synthesis and Molecular Modeling Studies. *J. Biomol. Struct. Dyn.* **2022**, *40* (22), 11495–11510.
- (12) Bortoleti, B. T. D. S.; Gonçalves, M. D.; Tomiotti-Pellissier, F.; Camargo, P. G.; Assolini, J. P.; Concato, V. M.; Detoni, M. B.; Biddóia, D. L.; Bispo, M. L. F.; Lima, C. H. D. S.; de Macedo, F. C., Jr; Conchon-Costa, I.; Miranda-Sapla, M. M.; Wowk, P. F.; Pavanelli, W. R. Investigation of the Antileishmanial Activity and Mechanisms of Action of Acetyl-Thiohydantoins. *Chem. Biol. Interact.* **2022**, *351*, No. 109690.
- (13) Camargo, P. G.; Bortoleti, B. T. da S.; Fabris, M.; Gonçalves, M. D.; Tomiotti-Pellissier, F.; Costa, I. N.; Conchon-Costa, I.; Lima, C. H. da S.; Pavanelli, W. R.; Bispo, M. de L. F.; Macedo, F., Jr Thiohydantoins as Anti-Leishmanial Agents: N Vitro Biological Evaluation and Multi-Target Investigation by Molecular Docking Studies. *J. Biomol. Struct. Dyn.* **2022**, *40* (7), 3213–3222.
- (14) Pereira, P. M. L.; Camargo, P. G.; Fernandes, B. T.; Flores-Junior, L. A. P.; Dias, L. R. S.; Lima, C. H. S.; Pingue-Filho, P.; Lioni, L. M. Y.; Yamada-Ogatta, S. F.; Bispo, M. L. F.; Macedo, F. In Vitro Evaluation of Antitrypanosomal Activity and Molecular Docking of Benzoylthioureas. *Parasitol. Int.* **2021**, *80* (October 2020), No. 102225.
- (15) Andriani, G. M.; de Almeida Spoladori, L. F.; Fabris, M.; Camargo, P. G.; Pereira, P. M. L.; Santos, J. P.; Bartolomeu-Gonçalves, G.; Alonso, L.; Lancheros, C. A. C.; Alonso, A.; Nakamura, C. V.; Macedo, F., Jr; Pingue-Filho, P.; Yamauchi, L. M.; de Lima Ferreira Bispo, M.; Tavares, E. R.; Yamada-Ogatta, S. F. Synergistic Antifungal Interaction of N-(Butylcarbamothioyl) Benzamide and

- Amphotericin B against Cryptococcus Neoformans. *Front. Microbiol.* **2023**, *14*, No. 1040671, DOI: 10.3389/fmicb.2023.1040671.
- (16) Camargo, P. G.; Fabris, M.; Silva, T. U.; Silva Lima, C. H.; Paula Machado, S.; Tonin, L. T. D.; Lima Ferreira Bispo, M.; Macedo, F. Thiohydantoins as Potential Antioxidant Agents: In Vitro and in Silico Evaluation. *ChemistrySelect* **2021**, *6* (38), 10429–10435.
- (17) Kang, L.; Gao, X.-H.; Liu, H.-R.; Men, X.; Wu, H.-N.; Cui, P.-W.; Oldfield, E.; Yan, J.-Y. Structure–Activity Relationship Investigation of Coumarin–Chalcone Hybrids with Diverse Side-Chains as Acetylcholinesterase and Butyrylcholinesterase Inhibitors. *Mol. Divers.* **2018**, *22* (4), 893–906.
- (18) Fabris, M.; Camargo, P.; Silva, M.; Silva, T.; Machado, S.; Rodrigues, C.; Lima, C.; Albuquerque, M.; Bispo, M. Exploring Urease Inhibition by Coumarin Derivatives through in Silico and in Vitro Methods. *J. Braz. Chem. Soc.* **2024**, *35*, No. 15, DOI: 10.21577/0103-5053.20230151.
- (19) Camargo, P. G.; Fabris, M.; Nakamae, M. Y. T.; de Freitas Oliveira, B. G.; da Silva Lima, C. H.; de Fátima, A.; de Lima Ferreira Bispo, M.; Macedo, F. Thiohydantoins and Hydantoins Derived from Amino Acids as Potent Urease Inhibitors: Inhibitory Activity and Ligand-Target Interactions. *Chem. Biol. Interact.* **2022**, *365*, No. 110045.
- (20) Jabri, E.; Carr, M. B.; Hausinger, R. P.; Karplus, P. A. The Crystal Structure of Urease from Klebsiella Aerogenes. *Science* (80-) **1995**, *268* (5213), 998–1004.
- (21) Brito, T. O.; Souza, A. X.; Mota, Y. C. C.; Morais, V. S. S.; De Souza, L. T.; De Fátima, A.; Macedo, F.; Modolo, L. V. Design, Syntheses and Evaluation of Benzoylthioureas as Urease Inhibitors of Agricultural Interest. *RSC Adv.* **2015**, *5* (55), 44507–44515.
- (22) Searle, P. L. The Berthelot or Indophenol Reaction and Its Use in the Analytical Chemistry of Nitrogen. A Review. *Analyst* **1984**, *109* (5), No. 549.
- (23) Gao, X.; Tang, J.; Liu, H.; Liu, L.; Liu, Y. Structure–Activity Study of Fluorine or Chlorine-substituted Cinnamic Acid Derivatives with Tertiary Amine Side Chain in Acetylcholinesterase and Butyrylcholinesterase Inhibition. *Drug Dev. Res.* **2019**, *80* (4), 438–445.
- (24) Lu, Q.; Chen, Y.; Liu, H.; Yan, J.; Cui, P.; Zhang, Q.; Gao, X.; Feng, X.; Liu, Y. Nitrogen-containing Flavonoid and Their Analogs with Diverse B-ring in Acetylcholinesterase and Butyrylcholinesterase Inhibition. *Drug Dev. Res.* **2020**, *81* (8), 1037–1047.
- (25) Camargo, P. G.; Fabris, M.; Tatsuta Nakamae, M. Y.; Germano de Freitas Oliveira, B.; Henrique da Silva Lima, C.; de Fátima, A.; de Lima Ferreira Bispo, M.; Macedo, F. Thiohydantoins and Hydantoins Derived from Amino Acids as Potent Urease Inhibitors: Inhibitory Activity and Ligand-Target Interactions. *Chem. Biol. Interact.* **2022**, *365*, No. 110045.
- (26) Copeland, R. A. Evaluation of Enzyme Inhibitors in Drug Discovery. A Guide for Medicinal Chemists and Pharmacologists. *Methods Biochem. Anal.* **2005**, *46*, 1–265.
- (27) Hansson, T.; Marelius, J.; Åqvist, J. Ligand Binding Affinity Prediction by Linear Interaction Energy Methods. *J. Comput. Aided. Mol. Des.* **1998**, *12* (1), 27–35.
- (28) Armarego, W. L. E.; Chai, C. L. L. *Purification of Laboratory Chemicals*, 5th ed.; Elsevier Science, 2003.
- (29) Kataria, R.; Khatkar, A. Molecular Docking, Synthesis, Kinetics Study, Structure–Activity Relationship and ADMET Analysis of Morin Analogous as Helicobacter Pylori Urease Inhibitors. *BMC Chem.* **2019**, *13* (1), No. 45.
- (30) Systèmes, D. *Biovia Discovery Studio 2016 Comprehensive Modeling and Simulations*. Dassault Systèmes, San Diego, 2016.
- (31) Verdonk, M. L.; Cole, J. C.; Hartshorn, M. J.; Murray, C. W.; Taylor, R. D. Improved Protein-Ligand Docking Using GOLD. *Proteins Struct. Funct. Bioinforma.* **2003**, *52* (4), 609–623.
- (32) DeLano, W. L. Pymol: An Open-Source Molecular Graphics Tool. *CCP4 Newslett Protein Cryst.* **2002**, *40* (1), 82–92.
- (33) Vanommeslaeghe, K.; Hatcher, E.; Acharya, C.; Kundu, S.; Zhong, S.; Shim, J.; Darian, E.; Guvench, O.; Lopes, P.; Vorobyov, I.; Mackerell, A. D. CHARMM General Force Field: A Force Field for Drug-like Molecules Compatible with the CHARMM All-Atom Additive Biological Force Fields. *J. Comput. Chem.* **2010**, *31* (4), 671–690.
- (34) Abraham, M. J.; Murtola, T.; Schulz, R.; Páll, S.; Smith, J. C.; Hess, B.; Lindahl, E. GROMACS: High Performance Molecular Simulations through Multi-Level Parallelism from Laptops to Supercomputers. *SoftwareX* **2015**, *1*–2, 19–25.
- (35) Gordon, J. C.; Myers, J. B.; Folta, T.; Shoja, V.; Heath, L. S.; Onufriev, A. H++: A Server for Estimating PKas and Adding Missing Hydrogens to Macromolecules. *Nucleic Acids Res.* **2005**, *33* (Web Server), W368–W371.
- (36) Mark, P.; Nilsson, L. Structure and Dynamics of the TIP3P, SPC, and SPC/E Water Models at 298 K. *J. Phys. Chem. A* **2001**, *105* (43), 9954–9960.
- (37) Yu, W.; He, X.; Vanommeslaeghe, K.; MacKerell, A. D. Extension of the CHARMM General Force Field to Sulfonyl-containing Compounds and Its Utility in Biomolecular Simulations. *J. Comput. Chem.* **2012**, *33* (31), 2451–2468.
- (38) da Silva, T. U.; Pougy, K.; de, C.; Albuquerque, M. G.; da Silva Lima, C. H.; Machado, S. de P. Development of Parameters Compatible with the CHARMM36 Force Field for [Fe 4 S 4] 2+ Clusters and Molecular Dynamics Simulations of Adenosine-5'-Phosphosulfate Reductase in GROMACS 2019. *J. Biomol. Struct. Dyn.* **2022**, *40* (8), 3481–3491.
- (39) Bussi, G.; Donadio, D.; Parrinello, M. Canonical Sampling through Velocity Rescaling. *J. Chem. Phys.* **2007**, *126* (1), No. 014101.
- (40) Parrinello, M.; Rahman, A. Polymorphic Transitions in Single Crystals: A New Molecular Dynamics Method. *J. Appl. Phys.* **1981**, *52* (12), 7182–7190.
- (41) Hess, B.; Bekker, H.; Berendsen, H. J. C.; Fraaije, J. G. E. M. LINCS: A Linear Constraint Solver for Molecular Simulations. *J. Comput. Chem.* **1997**, *18* (12), 1463–1472.
- (42) Darden, T.; York, D.; Pedersen, L. Particle Mesh Ewald: An N · log(N) Method for Ewald Sums in Large Systems. *J. Chem. Phys.* **1993**, *98* (12), 10089–10092.
- (43) Gomes, D. E. B.; da Silva, A. W.; Lins, R. D.; Pascutti, P. G.; A, S. HbMap2Grace. Software for Mapping the Hydrogen Bond Frequency. *Lab. Mol. Model. Dyn.* **2009**.
- (44) Humphrey, W.; Dalke, A.; Schulten, K. VMD: Visual Molecular Dynamics. *J. Mol. Graph.* **1996**, *14* (1), 33–38.
- (45) Kumari, R.; Kumar, R.; Lynn, A. G. mmpbsa—A GROMACS Tool for High-Throughput MM-PBSA Calculations. *J. Chem. Inf. Model.* **2014**, *54* (7), 1951–1962.
- (46) Weatherburn, M. W. Phenol-Hypochlorite Reaction for Determination of Ammonia. *Anal. Chem.* **1967**, *39* (8), 971–974.
- (47) Khan, J. A.; Wahab, A. tul.; Javaid, S.; Al-Ghamdi, M.; Huwait, E.; Shaikh, M.; Shafqat, A.; Choudhary, M. I. Studies on New Urease Inhibitors by Using Biochemical, STD-NMR Spectroscopy, and Molecular Docking Methods. *Med. Chem. Res.* **2017**, *26* (10), 2452–2467.
- (48) Ferreira, D. F. Sisvar: A Guide for Its Bootstrap Procedures in Multiple Comparisons. *Ciência e Agrotecnologia* **2014**, *38* (2), 109–112.